Lawrence Berkeley National Laboratory

Title

Leakage and Sepage of CO2 from Geologic Carbon Sequestration Sites: CO2 Migration into Surface Water

Permalink

https://escholarship.org/uc/item/7bj1977s

Authors

Oldenburg, Curt M.
Lewicki, Jennifer L.

Publication Date

2005-06-17

Leakage and Seepage of CO$_2$ from Geologic Carbon Sequestration Sites: CO$_2$ Migration into Surface Water

Curtis M. Oldenburg

Jennifer L. Lewicki

Earth Sciences Division
Ernest Orlando Lawrence Berkeley National Laboratory
Berkeley, CA 94720

June 17, 2005

DISCLAIMER

TABLE OF CONTENTS

This page left intentionally blank.

LIST OF TABLES

LIST OF FIGURES

This page left intentionally blank.

ABSTRACT

Geologic carbon sequestration is the capture of anthropogenic carbon dioxide (CO$_2$) and its storage in deep geologic formations. One of the concerns of geologic carbon sequestration is that injected CO$_2$ may leak out of the intended storage formation, migrate to the near-surface environment, and seep out of the ground or into surface water. In this research, we investigate the process of CO$_2$ leakage and seepage into saturated sediments and overlying surface water bodies such as rivers, lakes, wetlands, and continental shelf marine environments. Natural CO$_2$ and CH$_4$ fluxes are well studied and provide insight into the expected transport mechanisms and fate of seepage fluxes of similar magnitude. Also, natural CO$_2$ and CH$_4$ fluxes are pervasive in surface water environments at levels that may mask low-level carbon sequestration leakage and seepage. Extreme examples are the well known volcanic lakes in Cameroon where lake water supersaturated with respect to CO$_2$ overturned and degassed with lethal effects. Standard bubble formation and hydrostatics are applicable to CO$_2$ bubbles in surface water. Bubble-rise velocity in surface water is a function of bubble size and reaches a maximum of approximately 30 cm s^{-1} at a bubble radius of 0.7 mm. Bubble rise in saturated porous media below surface water is affected by surface tension and buoyancy forces, along with the solid matrix pore structure. For medium and fine grain sizes, surface tension forces dominate and gas transport tends to occur as channel flow rather than bubble flow. For coarse porous media such as gravels and coarse sand, buoyancy dominates and the maximum bubble rise velocity is predicted to be approximately 18 cm s^{-1}. Liquid CO$_2$ bubbles rise slower in water than gaseous CO$_2$ bubbles due to the smaller density contrast. A comparison of ebullition (i.e., bubble formation) and resulting bubble flow versus dispersive gas transport for CO$_2$ and CH$_4$ at three different seepage rates reveals that ebullition and bubble flow will be the dominant form of gas transport in surface water for all but the smallest seepage fluxes or shallowest water bodies. The solubility of the gas species in water plays a fundamental role in whether ebullition occurs. We used a solubility model to examine CO$_2$ solubility in waters with varying salinity as a function of depth below a 200 m-deep surface water body. In this system, liquid CO$_2$ is stable between the deep regions where supercritical CO$_2$ is stable and the shallow regions where gaseous CO$_2$ is stable. The transition from liquid to gaseous CO$_2$ is associated with a large change in density, with corresponding large change in bubble buoyancy. The solubility of CO$_2$ is lower in high-salinity waters such as might be encountered in the deep subsurface. Therefore, as CO$_2$ migrates upward through the deep subsurface, it will likely encounter less saline water with increasing capacity to dissolve CO$_2$ potentially preventing ebullition, depending on the CO$_2$ leakage flux. However, as CO$_2$ continues to move upward through shallower depths, CO$_2$ solubility in water decreases strongly leading to greater likelihood of ebullition and bubble flow in surface water. In the case of deep density-stratified lakes in which ebullition is suppressed, enhanced mixing and man-made degassing schemes can alleviate the buildup of CO$_2$ and related risk of dangerous rapid discharges. Future research efforts are needed to increase understanding of CO$_2$ leakage and seepage in surface water and saturated porous media. For example, we recommend experiments and field tests of CO$_2$ migration in saturated systems to formulate bubble-driven water-displacement models and relative permeability functions that can be used in simulation models.

This page left intentionally blank.

1. INTRODUCTION

Geologic carbon sequestration is the capture of anthropogenic CO$_2$ and its storage in deep underground formations such as depleted oil and gas reservoirs and deep brine-filled formations. The anthropogenic CO$_2$ that would otherwise be emitted into the atmosphere will typically be separated from industrial and power-plant flue gases. The purpose of geologic carbon sequestration is to reduce net atmospheric emissions of CO$_2$ to mitigate potential climate change associated with the role of CO$_2$ as a greenhouse gas.

One of the key issues associated with geologic carbon sequestration is the integrity of the geological reservoir with respect to containment of CO$_2$ for a significant although yet-to-be-defined time frame so that the strategy serves the intended purpose of reducing net CO$_2$ emissions. An additional concern is that leaking CO$_2$ from geologic sequestration sites may cause potential health, safety, and environmental (HSE) risks. We have investigated potential HSE risks in prior research through our modeling of CO$_2$ leakage and seepage in the near-surface environment (Oldenburg and Unger, 2003; 2004). In this previous work, we focused on CO$_2$ migration in the vadose zone of on-shore environments. However, geologic carbon sequestration is being implemented in off-shore environments such as in the Sleipner project (e.g., Torp and Gale, 2004), and many other off-shore projects are being discussed. Furthermore, CO$_2$ may seep into surface waters in on-shore environments prior to influencing the vadose zone or atmospheric surface layer. Consequently, there is a need to investigate CO$_2$ leakage and seepage in areas where CO$_2$ will seep into surface waters such as rivers, lakes, wetlands, and oceans in order to understand HSE risks in these environments.

To evaluate surface-water effects on CO$_2$ leakage and seepage, the following key research questions must be addressed: (1) What are the physical processes relevant to CO$_2$ migration through sediments and overlying surface water either as bubbles or as a dissolved component in water? (2) Does surface water attenuate or enhance CO$_2$ seepage flux? (3) Under what conditions can CO$_2$ concentrations build up at depth and lead to the potential for catastrophic release?

This project focuses on CO$_2$ seepage at relatively low fluxes in which liquid water is the connected phase and the CO$_2$ exists either in discrete bubbles or as a dissolved component in the aqueous phase. As will be shown, CO$_2$ in bubbles can be in gaseous, supercritical, and even liquid phases depending on the pressure and temperature in the surface or pore water. The salinity, temperature, and pressure (depth) span a wide range in surface- and pore-water systems. The surface-water bodies of interest are, in order of increasing depth, wetlands, rivers, lakes, and oceans. We also consider bubble rise in pore water in sediments and pore space in general immediately below surface water.

The purpose of this report is to summarize the state of knowledge of the transport of CO$_2$ through surface-water bodies and to a lesser extent through water-saturated sediments. In so doing, we will discuss the physical processes of ebullition and bubble flow as well as transport by diffusion and dispersion. We also discuss the implications of CO$_2$ seepage into surface water and subsequent bubble flow and transport on potential leakage and seepage fluxes from geologic carbon sequestration sites. This project was undertaken with a very limited budget and within a short time frame, and is therefore necessarily limited in scope.

2. DEFINITIONS AND ENVIRONMENT

2.1. Terminology

In this section, we discuss terminology and definitions to formalize the later discussion in the report. Table 2.1 shows key terms, definitions, and examples that apply to CO$_2$ leakage and seepage from geologic carbon sequestration sites, and the associated form of transport of CO$_2$ in surface water and subjacent saturated sediments. In Table 2.2, we present a categorization of some of the processes and conditions that tend to favor either ebullition or dispersion. We find that relatively low fluxes and high solubility of CO$_2$ in the surface water tend to favor dispersion, since bubbles will tend not to form. In contrast, relatively high fluxes and low solubility of CO$_2$ tend to favor ebullition and bubble flux upward. Secondary features such as bottom topography may also affect ebullition and dispersion by facilitating density-driven flow and associated mixing.

We present in Fig. 2.1 a schematic of the various ways that CO$_2$ seepage can occur from subjacent sediments to overlying surface water, with emphasis on the terminology of the process that occurs upon transition between these two environments. For example, in the first column of Fig. 2.1, transport is by advection and diffusion in the porous media, and by bubble flux in the surface water. The transition at the sediment-water interface occurs by the process of *ebullition*. Ebullition at the sediment-water interface could occur if CO$_2$ gas solubility in the surface water is less than in the pore water (e.g., if the surface water is more saline than the groundwater). In the second column, the transport is by bubble flux in both the sediments and the surface water. In the third column, transport is by advection and diffusion in both media. And finally, in the fourth column, transport is by bubble flux in the porous media, and by advection and diffusion in the surface water, the transition being caused by *dissolution* at the interface. Dissolution at the sediment-water interface could occur in cases where the groundwater is warmer than the surface water, in which case CO$_2$ solubility would increase upon reaching the cooler surface water.

Bubble transport in surface water is familiar to everyone from their experiences observing the behavior of CO$_2$ bubbles in carbonated beverages. The form of bubble flow in porous media is not as familiar to people, although fluidized beds and packed-bed reactors with upward gas flow are well-known chemical processing techniques (Iliuta et al., 1999). We limit our consideration to the case where the solid grains are not disturbed by the bubble flow, and we present in Fig. 2.2 a sketch of two different end-members within this regime: (1) discrete bubbles, and (2) channel flow. If the gas flux is low, gases can migrate upward through pore bodies and throats as small individual bubbles, with deformation and blockage occurring as controlled by solid matrix grains (Fig. 2.2a). In contrast, when the flux is large, gas bubbles can be larger and/or more numerous leading to greater entrapment and coalescence. When entrapment and coalescence exceed a threshold, a connected channel of gas forms between the leading edge of water displacement and the gas source. When this connectivity occurs, gas flow can be driven by gas-pressure-gradient rather than buoyancy forces, and these pressure-gradient forces can overcome the capillary, permeability, and/or liquid displacement resistances and displace water. Flow in a channelized regime is further favored by the low gas viscosity. Further details on bubble flow in porous media are presented in Sections 4.3 and 4.4.

Table 2.1. Definitions of terms used in this report.

Term	Definition	Example
Leakage	Migration in the subsurface away from the primary containment formation.	CO$_2$ escaping from the containment reservoir through an unrecognized permeable fault.
Seepage	Migration across a boundary such as the ground surface or into surface water.	CO$_2$ emissions from the ground into the atmosphere after leaking up a permeable fault.
Bubble	Immiscible volume of a secondary fluid phase (e.g., supercritical, gas, liquid) within a primary connected phase (e.g., aqueous) in which the bubble is contained.	CO$_2$ or CH$_4$ gas in surface water above seepage sites.
Ebullition	Formation of bubbles from a liquid supersaturated with respect to dissolved gases, either in surface water or in groundwater.	Concentrations of dissolved CO$_2$ or CH$_4$ in sediments below wetlands can reach supersaturation causing exsolution of gas bubbles.
Bubble flux	Flux of component as transported in discrete bubbles.	CO$_2$ in bubbles moving buoyantly upward in surface water.
Dissolution	Uptake of volatile components into solution in the liquid phase.	Carbonation of water produces CO$_2$ in solution in fresh water, as in carbonated drinks prior to degassing.
Advection	Component transport driven by movement of a phase containing the component.	CO$_2$ dissolved in water is transported along with the flowing water.
Diffusion	Component transport driven by concentration gradients within a phase.	Biogenic CO$_2$ or CH$_4$ in sediments below wetlands generated at a low rate creates concentration gradients of dissolved species that are then transported from high to low concentration (i.e., down the concentration gradient).
Dispersion	Component transport by small-scale advective motions and by diffusion that can be modeled collectively as a diffusive process.	CO$_2$ or CH$_4$ transported by turbulent motions and molecular diffusion induced by tidal flushing in wetlands.

Table 2.2. Factors favoring ebullition and dispersion.

Property	Favoring ebullition	Characteristic of …	Favoring dispersion	Characteristic of …
CO$_2$ seepage flux	Large, focused	High leakage rate	Small, diffuse	Low leakage rate
Currents	Stagnant, stable	Oceans, equatorial lakes	Mixed, unstable	Rivers, high-latitude lakes
Salinity	High, salty	Shallow inland seas	Low, fresh water	Rivers, lakes
Temperature	Warm	Estuaries, wetlands	Cold	High-latitude rivers, lakes, deep ocean
Depth	Shallow	Estuaries, wetlands, rivers	Deep	Oceans, mountain and crater lakes
Bottom topography	Flat, horizontal	Oceans, seas	Sloping, with relief	Rivers, lakes

2.2. Environment of Interest

The focus of this report is on CO$_2$ migration upward through saturated sediments and overlying surface water. The environments we consider are shown schematically in cross-section in Fig. 2.3. As shown, rivers, lakes, wetlands, estuaries, and continental shelf marine environments are within the scope of our discussion. Salinity, depth, temperature, and degree of mixing are all key characteristics that bear on the question of CO$_2$ transport. We consider the existence of non-specific leakage pathways upward from the deep CO$_2$ injection horizons as being capable of delivering CO$_2$ to the shallow environment. These leakage pathways could be along faults or fault zones, but we assume that by the time the CO$_2$ reaches the shallow sediments below surface water, the CO$_2$ flux is dispersed and relatively small. The reason for this focus is that large fluxes, e.g., from well blowouts, will be obvious HSE risks that will be mitigated as quickly as possible. Of more concern from the HSE perspective are small fluxes that may be hard to detect but that could lead to HSE consequences, either in the long-term, or due to near-surface buildup and rapid emission (e.g., Lake Nyos (Sigurdsson et al., 1987)). The seepage fluxes that we consider in our analysis of Section 4.5 are the same as used in our prior work (Oldenburg and Unger, 2003; 2004).

Within the range of pressures below the surface water bodies of interest, CO$_2$ can be in gaseous, supercritical, or liquid conditions. As shown in the phase diagram for pure CO$_2$ (Fig. 2.4), CO$_2$ has a critical point of 73.8 bars and 31.0 ^{o}C, and is a gas at ambient atmospheric temperature and pressure (1 bar, 25 ^{o}C). Shown on Fig. 2.4 is a wide band indicating a *P-T* path within the earth assuming a geothermal gradient of 25 ^{o}C km^{-1} and hydrostatic pressure. As shown, the *P-T* path passes almost directly through the critical point. In fact, in continental onshore conditions as we

have studied in the past (Oldenburg and Unger, 2003), the *P-T* path from depth to surface passes below the critical point. By such a path, CO$_2$ changes from supercritical to gaseous, and undergoes no large jumps in physical properties (e.g., density or viscosity) as it passes through 31 ^{o}C at pressures below 73.8 bars. In contrast, in the offshore or deep surface-water condition, the *P-T* path will traverse part of the liquid-stability field from depth to the surface because of the hydrostatic pressure in the surface water and lack of geothermal gradient there. In essence, the *P-T* path in the subsurface is shifted upward when there is surface water, and this causes the *P-T* path to intersect part of the liquid field. In Fig. 2.4, the top edge of the wide *P-T* path can be considered to be a sub-surface-water *P-T* path, and the bottom edge a sub-onshore-vadose zone path. The transition from gaseous to liquid CO$_2$ or vice versa is associated with strong changes in density, viscosity, and solubility with implications for CO$_2$ seepage into surface water as will be discussed in Section 4.6.

3. NATURAL CO$_2$ AND CH$_4$ FLUXES

3.1. Introduction

CO$_2$ leakage from geologic carbon sequestration sites, should it occur, will be superimposed on gas fluxes originating from a variety of biological and hydrological processes and sources. Numerous studies have been conducted to measure natural CO$_2$ and CH$_4$ fluxes, to estimate the relative contributions of ebullition and dispersion to the total flux, and to determine the physical processes controlling ebullition and dispersion. These studies offer direct evidence of how leakage and seepage fluxes of similar magnitude will behave in similar environments. We have discussed the issue of natural background gas fluxes with respect to the problem of detecting CO$_2$ leakage and seepage (Oldenburg and Lewicki, 2004). Below, we present a review of natural CO$_2$ and CH$_4$ fluxes relevant to developing an understanding of CO$_2$ leakage and seepage into surface water.

3.2. Groundwater

Recent studies have quantified the flux of CO$_2$ derived from deep crustal and mantle origin that is dissolved and transported by shallow groundwaters (e.g., Evans et al. 2002; Chiodini et al., 1999 and 2000). For example, throughout Tyrrhenian Central Italy, widespread non-volcanic CO$_2$ degassing (likely originating from a crustally-contaminated mantle or a mixture of magmatic and crustal components) occurs from vent and diffuse soil gas emissions and from CO$_2$-enriched groundwaters (Chiodini et al., 1999). From the Tyrrhenian Sea to the Apennine Mountains, buried structural highs act as gas traps. When total pressure of the reservoir fluid exceeds hydrostatic pressure, a free gas phase forms gas reservoirs from which gas may escape to the surface. Carbon dioxide is then released to the atmosphere either directly through gas emissions or by dissolution in groundwaters and subsequent release at surface springs. Measured CO$_2$ partial pressure (P_{CO2}) values for springs are up to four orders of magnitude greater than that of the atmosphere (Chiodini et al., 1999). Therefore, when groundwater is discharged at the surface, it releases a large amount of the carbon through CO$_2$ degassing. Chiodini et al. (1999, 2000) found that in geographic regions characterized by thick regional carbonate aquifers, most or part of the deeply derived gas is dissolved by the aquifers, whereas in

regions characterized by small aquifers, these aquifers cannot dissolve a large quantity of the CO$_2$ and extensive vent and soil CO$_2$ emissions occur at the surface. Chiodini et al. (2000) used mass balance equations coupled with carbon isotopic analyses and hydrologic data to estimate the flux of deeply derived CO$_2$ into the aquifers. These authors estimated deeply derived CO$_2$ fluxes up to 0.29 g m^{-2} d^{-1} into the carbonate Apennine aquifers. For high P_{CO2} waters, the CO$_2$ flux lost to the atmosphere is of the same order of magnitude as the influx of deep CO$_2$**.**

Evans et al. (2002) conducted a chemical, isotopic, and hydrologic investigation of cold springs around Mammoth Mountain, California, USA. Based on these data, they estimated that the cold groundwater system around Mammoth Mountain discharges ~2 x 10^4 tonnes y^{-1} of magmatic carbon (as CO$_2$), indicating that these waters have the ability to dissolve and transport large quantities of deeply derived CO$_2$. They also interpreted the 1 x 10^5 tonnes CO$_2$ y^{-1} that degasses diffusely through soils at Mammoth to be the gas that exceeds the dissolving capacity of the groundwater.

Shipton et al. (2004a, b) investigated the northern Paradox Basin (Utah, USA) as a natural analog for CO$_2$ leakage from a geologic carbon storage reservoir. Here, CO$_2$ of deep-crustal origin leaks from numerous storage reservoirs (high P_{CO2} shallow aquifers) along faults to the surface. An important loss of CO$_2$ to the atmosphere occurs as groundwaters discharge as springs at the surface and CO$_2$ degasses, as is evidenced by continual bubbling of CO$_2$ from many of these springs (Shipton et al., 2004a, b).

3.3. Wetlands

Much attention has focused on understanding the origin, transport, and fate of CH$_4$ in wetlands (e.g., Harriss and Sebacher, 1981; Wilson et al., 1989; MacDonald et al., 1998; Walter and Heimann, 2000; Rosenberry et al., 2003; Christensen et al., 2003) because these regions contain large quantities of stored organic carbon that, if released as CH$_4$, may strongly influence global climate. Wilson et al. (1989) showed from repeated measurements of CH$_4$ flux in a temperate freshwater swamp that this flux was highly variable over space and time. Ebullition from the bottom sediments was an important form of CH$_4$ release; although ebullition was only recorded in 19% of their measurements, it accounted for 34% of the total flux over time. However, unlike many other studies, they found that flux was not correlated with water depth. Rosenberry et al. (2003) presented hydraulic-head data for a peatland in northern Minnesota, USA, which indicated that the peatland was overpressured at depth and the amount of overpressuring varied over time. This temporal variability was indicative of changes in the volume of gas bubbles in the peat column in response to changes in temperature, and rates of gas production, transport, phase change, and ebullition. The numerous rapid declines observed in overpressuring were likely caused by ebullition events, which occur to reduce the pressure-head difference with a decrease in water level (Rosenberry et al., 2003). Christensen et al. (2003) measured in a closed laboratory system diffusion and ebullition fluxes of CH$_4$ from monoliths taken from wetland ecosystems in Sweden. They showed that ebullition accounts for 18 to 50% of the total CH$_4$ flux from their system and that this may represent a minimum contribution expected in nature, due to the stable laboratory conditions (e.g., isothermal, no wind).

3.4. Rivers

Smith et al. (2000) measured both diffusive and bubbling CH$_4$ fluxes in open water, bare soils, macrophyte mats, and flooded forest along the Orinoco River floodplain, Venezuela. They found that due to productivity, the flooded forest environment accounted for the highest diffusive and bubble fluxes and that ebullition accounted for 65% of all emissions. Large temporal variations in CH$_4$ fluxes were also observed, due primarily to seasonally fluctuating water levels. The diffusive CH$_4$ flux was constant over the seasons in the open water environment, but ebullition was higher during dry seasons.

Where the Little Grand Wash Fault Zone crosses the Green River (Utah, USA), CO$_2$ of deep-crustal origin discharges into the Green River. Here, a line of gas bubbles is observed along the fault trace (e.g., Shipton et al., 2004a, b).

3.5. Lakes and Reservoirs

Numerous investigations have focused on describing and quantifying the production and transport of CH$_4$ and CO$_2$ in lakes and reservoirs (e.g., Sigurdsson et al., 1987; Oskarsson, 1990; Giggenbach, 1990; Giggenbach et al., 1991; Keller and Stallard, 1994; Woods and Philips, 1999; Casper et al., 2000; Joyce and Jewell, 2003). In non-volcanic/magmatic lake environments, CO$_2$ and CH$_4$ are primarily derived from biologic processes. The primary pathways of gas exchange between water and the atmosphere are molecular diffusion across the air-water interface and ebullition from the sediment through the water column. Pathways of exchange of CO$_2$ and CH$_4$ between the lake and the atmosphere differ significantly because of their different solubilities, different concentrations in the epilimnion, and different atmospheric concentrations. Because the solubility of CH$_4$ in water is about an order of magnitude less than that of CO$_2$ (20 $^{\circ}$C), elevated CH$_4$ concentrations at depth lead to bubble formation, whereas elevated aqueous CO$_2$ concentrations can build up at depth. Many lakes are supersaturated with respect to CO$_2$, particularly in the wintertime, when productivity, and therefore photosynthetic uptake, is low. Ebullition is the primary release mechanism of methane from lakes and other shallow water environments (i.e., where CH$_4$ production is high and water is shallow). However, bubbling is episodic and dependent on a variety of factors such as temperature, water depth, barometric pressure variations, winds, and related bottom shear stress (e.g., Keller and Stallard, 1994; Walter and Heimann, 2000; Rosenberry et al., 2003; Joyce and Jewell, 2003).

Casper et al. (2000) measured CO$_2$ and CH$_4$ concentration gradients with depth in a small freshwater lake in the U.K. and determined the diffusion and ebullition fluxes of CH$_4$ and CO$_2$ to the atmosphere. They found that ebullition accounted for 96% of the CH$_4$ flux and diffusion accounted for 99% of the CO$_2$ flux. The rate of gas ebullition was highly variable in space and time and decreased with water depth. Casper et al. (2000) also observed pulses of ebullition to be correlated with periods of falling barometric pressure. Joyce and Jewell (2003) estimated the contribution of bubble to total methane flux, its temporal variation, and relationship to current velocities at several lakes in Panama and Puerto Rico. The authors found a correlation between current velocity and CH$_4$ flux and also observed temporal correlation of bubbling across sites in the lakes. They proposed a physical model relating lake-bottom shear stresses to measured current velocities, whereby sediments can be sheared only by bottom currents that are able to overcome the sediment cohesive strength. When this occurs, ebullition is induced. However, the magnitude of ebullition flux depends not only on threshold shear velocity but also on the

quantity of the free gas in the sediments available for release. As a result, large bubbling events may occur without trigger after prolonged periods of quiescence because substantial methane has accumulated. Conversely, no bubbling may occur with significant current velocities if no gas has accumulated (Joyce and Jewell, 2003).

Much attention has been paid to the transport and fate of CO$_2$ in lakes in volcanic/magmatic environments, due to the lethal gas bursts that occurred at Lakes Monoun and Nyos, Cameroon, in 1984 and 1986, respectively. Approximately 1800 people were killed in these combined events by the hypothesized overturn and depressurization of CO$_2$-rich lake waters (derived from emission of magmatic CO$_2$ into the lakes) and subsequent large-scale CO$_2$ ebullition. Lake-overturn has been suggested to be caused by wind-driven mixing, precipitation, and landslides. However, the viability of these triggering mechanisms has remained unclear. Regardless of this uncertainty, these lakes displayed density stratification and within the deep anoxic stagnant layers, P_{CO2} built up to equal the ambient hydrostatic pressure (Sigurdsson et al., 1987; Oskarsson, 1990; Giggenbach, 1990). Under normal conditions, CO$_2$ may have diffused into shallow waters and escaped gradually to the atmosphere as bubbles formed at shallow water levels. However, the rapid overturn of these lakes caused depressurization of CO$_2$-rich deep waters and nucleation of CO$_2$ in the deep water. The resultant ebullition led to the gas bursts at the surface (Sigurdsson et al., 1987; Oskarsson, 1990; Giggenbach, 1990). In the Lake Nyos event, 240,000 tonnes of CO$_2$ were lost from the upper 100 m of the lake (Giggenbach, 1990). Giggenbach et al. (1991) showed that other CO$_2$-rich lakes worldwide (Laacher See, Germany, Dieng, Indonesia, and Mt. Gambier, Australia) display similar chemical and physical characteristics to Lakes Nyos and Monoun. In general, seasonal overturn, other periodic deep mixing processes, or man-made degassing schemes (e.g., Halbwachs et al., 2004) are needed to prevent density stratification and the potential for extreme buildup of CO$_2$ at depth in lakes subject to CO$_2$ influxes at depth.

3.6. Marine Environments

Hoveland et al. (1993) presented a review of CH$_4$ degassing from shallow marine sediments worldwide and estimated the global flux. Based on geophysical mapping, visual observations, and geochemical sampling, CH$_4$ occurs at aqueous saturation concentrations and in free gas form at many locations in the upper layers of marine sedimentary basins (Hoveland et al., 1993 and references therein). This CH$_4$ originates either from microbial degradation of organic material in shallow sediments or at greater depth in sedimentary basins (> 2 km) by thermal "cracking" of organic materials to form petroleum hydrocarbons. Methane may then migrate by diffusion in pore waters or as bubbles. In many locations, gas escapes from shallow marine sediments to the water column as continuous or intermittent bubble streams (Hoveland et al., 1993 and references therein). For example, in the Gulf of Mexico, gas seeps are associated with different geological environments (e.g., deltaic sediments, salt domes, and gas hydrates in sediments on and at the base of the continental slope) (Anderson and Bryant, 1990). In the North Sea, gas migrates from depth along deep-seated faults and evidence of gas (acoustic turbidity) close to the seabed is present over an area of ~120,000 m^2. Within this larger area, ~120 bubble plumes within a 6500 m^2 area have been observed. At Cape Lookout Bight, a marine basin on the Outer Banks of North Carolina, USA, shallow sediment pore waters become saturated with methane during the summer and ebullition occurs during low tide due to reduction in hydrostatic pressure (Martens and Klump, 1980). Martens and Klump (1980) estimated that ~15% of the methane in the

bubbles here is lost to solution during transit through the water column and ~6.9 x 10^7 g CH$_4$ yr^{-1} are lost to the atmosphere.

Perhaps the most well studied and quantified hydrocarbon ebullition in shallow marine environments has occurred near Coal Oil Point, off the coast of Santa Barbara, California, USA (e.g., Hornafius et al., 1999; Leifer et al., 2000; Washburn et al., 2001; Boles et al., 2001). This area hosts one of the most prolific hydrocarbon seep fields in the world, where extensive, dense bubbling plumes emit from faults and fractures along the axes of anticlinal hydrocarbon traps. Based on sonar data, Hornafius et al. (1999) estimated that the total emission rate of hydrocarbons into the water column through ebullition was 1.7 ± 0.3 x 10^5 m^3 d^{-1} (18 km^2 area). Leifer et al. (2000) measured the bubble gas partial pressures, dissolved gas and oil, and fluid motions within the rising bubble streams of shallow (<70 m) seeps. They found that near-surface aqueous methane concentrations were >10^8 times greater than atmospheric equilibrium values. Also, they demonstrated how large seeps can modify the local environment by generating upwelling flows, turbulence, and saturating the water contained within the bubble plume with CH$_4$. Therefore, the fraction of gas that is released to the atmosphere versus dissolved in the water column depends both on the seep itself and the above bubble stream environment (Leifer et al., 2000). Boles et al. (2001) monitored gas flow rates from a large seep (67 m depth) where gas is captured by two steel tents and piped to shore to be processed. They observed that tidal forcing caused gas flow rate to vary by 40% around the average flow rate and high and low tides were correlated with reduced and increased flow rates, respectively. Boles et al. (2001) proposed a pore activation model to explain these observations, where gas bubbles are released from small pores at low pressures but at high pressures, ebullition is inhibited.

4. CO$_2$ LEAKAGE AND BUBBLE FLOW

4.1. Bubble Formation Fundamentals

In order for a bubble to form and persist in water, the pressure within the bubble must be greater than the ambient hydrostatic pressure plus the surface tension of water that must be overcome to form the bubble. Mathematically, the pressure inside the bubble (P) is equal to the sum of the partial pressures of the volatile species which must be in excess of the sum of the ambient hydrostatic pressure at depth z (P_z) and the surface tension pressure (P_{st}):

$$P = \sum_i C_i H_i > P_z + P_{st} \qquad\qquad (4.1)$$

where H_i are the Henry's law coefficients (Pa or atm) for each species i, C_i are the aqueous concentrations of the volatile species (mole fractions), and the fluid pressure at depth z is given by

$$P_z = P_A + \rho_w\, g\, z \qquad\qquad (4.2)$$

where ρ_w is water density, g is gravity, and P_A is atmospheric pressure. A schematic of the radially outward surface forces and the tangential surface tension forces on a neutrally buoyant

single bubble is shown in Fig. 4.1. The P_{st} in Eq. 4.1 is related to the bubble radius (r) and the surface tension (σ) of the water according to the Young-Laplace equation (e.g., Pellicer et al., 2000) as

$$P_{st} = \frac{2\sigma}{r} = P - P_z \qquad (4.3).$$

Surface tension for water is approximately 72 dynes cm^{-1} (0.072 N m^{-1}), which means that P_{st} is negligible relative to P_z for bubbles with radius larger than approximately 150 μm (0.15 mm) for which $2\sigma/r \sim 0.1$ bar (e.g., Leifer and Patro, 2002).

The surface tension pressure (P_{st}) implies that the gas pressure in the bubble must be higher than the gas saturation pressure in the ambient aqueous phase. The bubble gas-phase composition is determined by the relative magnitude of the gas partial pressures and thus reflects the volatility (the inverse of the component's aqueous-phase solubility) of each species and the water composition. This relationship of ebullition to solubility is a key factor in CO$_2$ leakage because waters with varying solubility due to different salinity and temperature may be encountered during the long rise upward of CO$_2$ bubbles. The solubility and buoyancy of CO$_2$ over a potential migration path will be discussed below in Section 4.7.

Once a bubble is formed and rises upwards, it can exchange mass with the surrounding water. The bubble molar flux to surrounding water, F_i, is expressed as:

$$F_i = \frac{dN_i}{dt} = q_{Bi} 4\pi r^2 \left(C_i - \frac{P_{Bi}}{H_i} \right), \qquad (4.4)$$

(e.g., Leifer and Patro, 2002) where N_i is the molar content of gas species i in the bubble, q_{Bi} is the individual bubble gas transfer rate, and P_{Bi} is the bubble gas partial pressure.

Equation (4.4) is applied to each gas species in the bubble individually. The gas flux is driven by the difference $C_i - P_{Bi}/H_i$ (e.g., Leifer et al., 2000). Therefore, gas outflows from the bubble when $C_i < P_{Bi}/H_i$ and inflows when $C_i > P_{Bi}/H_i$. In the case of a bubble composed predominantly of CO$_2$, it will dissolve as CO$_2$ outflows and grow as dissolved air (primarily N$_2$ and O$_2$) and/or CO$_2$ inflow. If for example, C_{CO2} is elevated due to bubble dissolution, the gas outflow from the bubble is decreased. If concentrations of dissolved O$_2$ and N$_2$ in the water column are low, inflow will be reduced and dissolution will occur. With rise through the water column, CO$_2$ may dissolve and the bubble may shrink, increasing P_{ST} as the bubble radius decreases (see Eq. 4.3). Also, bubble expansion will occur due to decreasing P_z and associated gas expansivity. Upon rising and increasing in size, the larger bubble will be able to transfer gas more efficiently because of the increased surface area. The total gas entering the water column from rising bubbles depends on the cumulative integrated bubble molar flux over the bubble's lifetime.

So far we have implicitly assumed that the bubble in question is a gas bubble. However, for applications involving CO$_2$ rising from the deep subsurface during potential leakage from geologic carbon sequestration sites, the CO$_2$ can be in either a supercritical or liquid phase as well as a gas phase, depending on pressure and temperature (see Section 4.5, below). Much of the above fundamentals apply also for these cases in which the bubble contains supercritical or liquid phase CO$_2$, in which case we would refer to an equilibrium between species that paritition between the two liquid phases, aqueous and CO$_2$.

4.2. Steady-State Bubble Rise in Surface Water

Assuming that the bubble persists throughout its rise through the surface-water body, the bubble lifetime can be derived from the water-body depth divided by the bubble rise velocity. The velocity of bubble rise is often given by Stoke's law:

$$v = d^2 g \left(\frac{\rho_w - \rho_g}{18 \mu_w} \right) \tag{4.5}$$

where d is bubble diameter, ρ_w and ρ_g are water and gas density, respectively, and μ_w is water viscosity. By this well-known equation, the bubble velocity is directly related to the square of bubble diameter. Therefore, as P_z decreases, d increases and bubbles accelerate. However, Eq. 4.5 is only valid at very small Reynolds number (Re $= \rho_w\, v\, d/\mu_w < \sim 1$) corresponding to either very small bubble size, small buoyancy contrast, or a very viscous liquid. For CO$_2$ bubbles in surface water, Re is of order 1 when bubble diameter is of order 10^{-4} m (0.1 mm). In summary, Eq. 4.5 is a poor predictor of gas bubble rise velocity in surface water except for very small bubbles.

A wealth of empirical data from experiments and field measurements has provided a sound basis for estimating bubble rise velocity. We present in Fig. 4.2 a figure from Leifer and Patro (2002) showing data from experiments of bubble rise velocity as a function of bubble radius, with contours of Reynolds number (dashed lines). As shown, Eq. 4.5 applies only in the lowermost left-hand corner at Re < 1, and furthermore the rate of bubble rise in water has a maximum of approximately 30 cm s^{-1} which is reached when the bubble diameter is approximately 1.5 mm (r = 0.75 mm). Bubbles are known to begin oscillating at radii of approximately 0.7 mm and Re of 400, leading to a decrease in rise velocity as bubble radius increases. While these results are valid strictly for air bubbles, very similar results would be obtained for pure CO$_2$ gas bubbles since the driving force is given by the difference in density between the gas phase and water, a negligible difference when comparing the buoyancy of air ($\rho = 1.2$ kg m^{-3}) to gaseous CO$_2$ ($\rho =$ 1.8 kg m^{-3}) for bubbles in water ($\rho = 1000$ kg m^{-3}) at near-surface conditions.

4.3. Bubble and Channel Flow

Within a water-saturated porous medium such as the sediments or fractured rock below a surface-water body, upward buoyancy forces will act on CO$_2$ bubbles. However, within porous media, bubble flow is restricted by the presence of solid matrix grains and the tortuous path around them. In addition, capillary forces can arise from (1) contact of the bubble with the solid grains, and (2) the deformation of the bubble and corresponding change in bubble radius (r) (see Eq. 4.3) that occurs when the bubble squeezes through narrow pore throats. Pore throats can also lead to straining and trapping processes that block bubble flow (e.g., Wan et al., 2003). Bubble rise in porous media is therefore significantly more complicated than bubble rise in standing surface water.

The additional complexity of capillary forces due to the solid matrix grains can be quantified by reference to the Bond number (Bo), the ratio of buoyancy forces driving upward flow to surface tension forces that tend to retard bubble flow. The Bond number can be defined as

$$\text{Bo} = \frac{(\rho_w - \rho_g)g\,r_p^{\,2}}{\sigma} \qquad\qquad (4.6)$$

(e.g., Brooks et al., 1999) where r_p is a characteristic length scale of the pore space. When Bo > 1, buoyancy forces dominate, and when Bo < 1, capillary forces dominate. Taking values of ρ_w, ρ_g, g, and σ of 1000 kg m^{-3}, 1.8 kg m^{-3}, 9.81 m s^{-2}, and 7.2 x 10^{-2} N m^{-1}, respectively, we find that capillary forces will dominate for pore sizes less than approximately 3 mm. Capillarity will therefore be the important force in medium and fine-grained porous media. A modified Bond number can be defined to include pore body and pore throat length scales to account for the fact that buoyancy is more important in pore bodies, while capillarity is more important in pore throats (Brooks et al., 1999).

The Bond number can be used to classify whether gas flow in saturated porous media will occur by bubble or by channel flow (Brooks et al., 1999). Bubble flow occurs when buoyancy forces dominate and gravity drives gas bubbles upward without large capillarity effects. Such flow will occur when the porous media are coarse, such as in gravels and coarse sands. In contrast, fine porous media give rise to stronger capillary forces as gas is squeezed through small pore throats leading to gas becoming trapped by capillarity. As trapped gases accumulate in the medium, eventually they may form connected paths to the gas source area and pressure-driving forces can be propagated from the source to the gas-liquid front. At this point, gravity is aided by the pressure-gradient driving force and capillary forces can be overcome leading to water displacement as gas advances upward. If snap-off occurs isolating the leading gas-phase region from the gas source, capillarity can again stop the rise of the gas bubble. In this way, the rise of gas in medium and fine-grained porous media typically occurs only by channel flows in which elongated regions of gas flow upward in a gas channel (see Fig. 2.3). This has been observed in experimental studies of upward air flows in the field of air sparging (e.g., Ji et al., 1993). (Air sparging is a remediation technique in which air is injected into the ground so that it will bubble upwards capturing volatile contaminants from water as the air migrates upward.) Beyond the theoretical considerations of the Bond number, formation heterogeneity inherent in the subsurface can also control channel-formation.

4.4. Steady-State Bubble Rise in Porous Media

One recent analysis relevant to this study is that of Corapcioglu et al. (2004) who considered the problem of bubble rise velocity in porous media. Their study was a follow-on to an experimental study (Roosevelt and Corapcioglu, 1993) which was motivated by the need to understand air movement in air sparging. Along with a theoretical analysis of bubble rise in porous media, Corapcioglu et al. (2004) present an excellent review of prior studies of porous media bubble transport to which we refer interested readers. Here we present the development of Corapcioglu et al. (2004) and use it to predict CO$_2$ bubble rise velocity in porous media for both gaseous and liquid CO$_2$. We note that this analysis is valid only for single-bubble rise in coarse sediments, i.e., Bo > 1.

The analysis begins by considering the forces acting on a single bubble in a porous medium as shown in Fig. 4.3. For a bubble rising at steady-state, the upward buoyancy forces are exactly balanced by the surface tension and drag forces that tend to retard motion. These forces can be written as the buoyancy force, given by

$$F_b = \left(\rho_f - \rho_g\right)g\, \frac{4}{3}\pi\, R_b^{\,3} \tag{4.7},$$

the surface tension force given by

$$F_{st} = 2\pi R'\sigma \sin\theta \tag{4.8},$$

where R' is an equivalent pore throat radius, and the drag force is given by

$$F_d = A\left[\frac{150\,\mu_b u_b \left(1-n\right)^2}{d_p^{\,2}\, n^3} + \frac{1.75\rho_g u_b^{\,2}\left(1-n\right)}{d_p\, n^3}\right]\frac{4}{3}\pi\, R_b^{\,3} \tag{4.9}$$

(variables are defined in Nomenclature). The first term in brackets in Eq. 4.9 is the Kozeny term, accounting for viscous drag in laminar flow, while the second term is the Burke-Plummer term, accounting for turbulent losses. Summing these three forces and allowing for acceleration of the bubble, we have the balance relation

$$F_b - F_d - F_{st} = A_d\,\rho_g\,\frac{4}{3}\pi\, R_b^{\,3}\left(\frac{\partial u_b}{\partial t} + u_b\,\frac{\partial u_b}{\partial x}\right) \tag{4.10}$$

where the A_d term accounts for entrained liquid ahead of the bubble and is defined as

$$A_d = 1 + C_M\,\frac{\rho_f}{\rho_g} \tag{4.11}.$$

Substituting the individual force equations and grouping terms by the powers of bubble rise velocity (u_b), we obtain

$$-\left(C_1 u_b^2 + C_2 u_b + C_3\right) = \frac{\partial u_b}{\partial t} + u_b\,\frac{\partial u_b}{\partial x} \tag{4.12}$$

where

$$C_1 = \frac{1.75\left(1-n\right)A}{d_p\, n^3\, A_d} \tag{4.13}$$

$$C_2 = \frac{150\left(1-n\right)^2 A\,\mu_b}{d_p^{\,2}\, n^3\,\rho_g\, A_d} \tag{4.14}$$

$$C_3 = \frac{1}{\rho_g\, A_d}\left[\frac{3}{2}\frac{R'\sigma \sin\theta}{R_b^3} - \left(\rho_f - \rho_g\right)g\right] \tag{4.15}.$$

The rise velocity (u_b) can be calculated using the coefficients of Eqs. 4.13-4.15 in the quadratic equation 4.12 for which we assume steady state and zero inertia, i.e., right-hand side of Eq. 4.12 is set to zero. The values of the various terms in the above equations are given in Table 4.1, where we have included some additional sediment particle sizes and porosities to extend the method toward finer grain sizes than the 4 mm glass beads used in Roosevelt and Corapcioglu (1993). Many assumptions are made in the analysis, such as constant contact angle, bubble radius, and fit parameter for which we refer interested readers to Corapcioglu et al. (2004) for further information.

We have calculated bubble rise velocities for the 4 mm glass beads of Corapcioglu et al. (2004) and two slightly finer grain sizes (d_p = 2 mm and 1 mm) (see Table 4.2). We note that the approach breaks down for medium and fine grain sizes as evidenced by the negative rise velocity produced as a solution to the quadratic equation (Eq. 4.12). This is to be expected since this analysis is for bubble flow rather than channel flow which will occur for medium and fine grain sizes (see Section 4.2). Results are shown in Fig. 4.4 where we have plotted the logarithm of the calculated bubble-rise velocities for three coarse grain sizes (d_p = 4 mm, 2 mm, and 1 mm) for air and CO$_2$ gas bubbles, along with the calculated rise velocity for a CO$_2$ liquid bubble. The maximum velocity plotted is approximately 18 cm s^{-1}, which is considered by Corapcioglu et al. (2004) to be the maximum possible porous media bubble rise velocity, and is approximately one-half of the maximum surface-water bubble rise velocity (cf. Fig. 4.2). Note from Fig. 4.4 that for the 4 mm grain size, the CO$_2$ bubble is predicted to rise slightly slower than the air bubble, but that CO$_2$ bubbles are predicted to rise slightly faster than air bubbles for the less-coarse media. This cross-over effect is due to the greater buoyancy of air relative to CO$_2$ and its importance in coarse media, and the greater importance of the lower viscosity of CO$_2$ relative to air in finer media. Note finally that CO$_2$ liquid bubbles rise more slowly due to their greater density and viscosity than CO$_2$ gas bubbles. The main conclusion of this analysis is that the density contrast between air and CO$_2$ is negligible in the analysis of bubble rise velocity because buoyancy is generated by the density difference between the gas and water, and this difference is nearly the same because water density is nearly 1000 times larger than the gas density. However, liquid CO$_2$ density is much larger and liquid CO$_2$ bubbles are correspondingly much less buoyant in water. Despite the numerous simplifying assumptions in this analysis, the calculations reveal the importance of grain size, and density and viscosity contrast in predicting bubble rise velocity in coarse porous media. As for medium and fine porous media, gas flow will be by channel flow which can be analyzed by a wide range of multiphase reservoir simulation methods beyond the scope of the present project.

Table 4.1. Fluid properties for the analysis of bubble flow in porous media.

Property	Symbol	Value	Units
Surface tension	σ	7.2×10^{-2}	$N\ m^{-1}$
Contact angle	q	30	degrees
Viscosity of water	μ_w	1×10^{-3}	$kg\ m^{-1}\ s^{-1}$
Density of water	ρ_w	1000.	$kg\ m^{-3}$
Viscosity of air	μ_g	1.80×10^{-5}	$kg\ m^{-1}\ s^{-1}$
Density of air	ρ_g	1.2	$kg\ m^{-3}$
Viscosity of CO_2 Gas (1 bar, 20 ^{o}C) Liquid (61 bars, 22 ^{o}C)	 μ_g μ_l	 1.47×10^{-5} 6.33×10^{-5}	 $kg\ m^{-1}\ s^{-1}$ $kg\ m^{-1}\ s^{-1}$
Density of CO_2 Gas (1 bar, 20 ^{o}C) Liquid (61 bars, 22 ^{o}C)	 ρ_g ρ_g	 1.8 755.2	 $kg\ m^{-3}$ $kg\ m^{-3}$
Gravitational accel.	g	9.81	$m\ s^{-2}$
Additional mass	A_d	*1*	-
Fit parameter	A	26.8	-

Table 4.2. Porous media properties and results for bubble flow in porous media.

Property	Symbol	Units	4 mm glass beads[1]	Gravelly sand[2]	Coarse sand[2]
Porosity	*n*	-	0.3954	0.3	0.35
Particle size	d_p	*m*	*4 x 10^{-3}*	2 x 10^{-3}	1 x 10^{-3}
Bubble radius	R_b	*m*	*4 x 10^{-3}*	2 x 10^{-3}	1 x 10^{-3}
Equivalent pore throat radius	*R'*	m	*3.09 x 10^{-4}*	1.55 x 10^{-4}	7.73 x 10^{-5}
Rise velocity					
Air	u_b	m s^{-1}	1.83 x 10^{-1}	2.52 x 10^{-2}	7.73 x 10^{-3}
CO$_2$ Gas	u_b	m s^{-1}	1.68 x 10^{-1}	2.91 x 10^{-2}	9.40 x 10^{-3}
CO$_2$ Liquid	u_b	m s^{-1}	4.43 x 10^{-3}	8.60 x 10^{-4}	N/A
Burke-Plummer Permeability	*k*	m^2	1.80 x 10^{-8}	1.47 x 10^{-9}	6.76 x 10^{-10}

[2] de Marsily (1986)
[1] Corapcioglu et al. (2004)

4.5. Transport by Bubble Flow and Diffusion in Surface Water

To examine ebullition and diffusion rate, we consider a surface-water system consisting of air (N$_2$ and O$_2$), CO$_2$, and CH$_4$ similar to that described by Morel and Herring (1993). If seepage of CO$_2$ and/or CH$_4$ occurs across the sediment surface at depth *z* into the overlying surface water body at a constant flux, *m* (mol cm^{-2} s^{-1}), we can estimate the rates of ebullition and diffusion of these species. The following assumptions will be made: (1) bubble formation maintains the sum of the partial pressures (CO$_2$, CH$_4$, air, H$_2$O) at P_z, i.e., we neglect P_{st}, (2) bubbles rise so fast through the water column to the surface that no dissolution occurs, (3) transport of all solutes in the water column is described by a dispersion coefficient ($D = 10^{-3}$ cm^2 s^{-1}), and (4) chemical reactions (e.g., bicarbonate formation from CO$_2$, oxidation of CH$_4$) are ignored.

For each species, the rate of ebullition E_i (mol cm^{-2} s^{-1}) is proportional to its partial pressure at the sediment surface:

$$E_i = \frac{P_i}{P_z} E \qquad (4.17)$$

where E is the total rate of ebullition of all species together. A steady-state mass balance equation is written for each species at the sediment surface where the sum of its transport by diffusion and ebullition is equal to its rate of formation at depth:

$$\frac{D}{z}\left([CO_2]_b - [CO_2]_s\right) + EK_{CO2}^{-1}[CO_2]_b P_z^{-1} = m \qquad (4.18)$$

$$\frac{D}{z}\left([CH_4]_b - [CH_4]_s\right) + EK_{CH4}^{-1}[CH_4]_b P_z^{-1} = m \qquad (4.19)$$

$$\frac{D}{z}\left([air]_b - [air]_s\right) + \frac{E[air]_b}{K_{air}P_z} = 0 \qquad (4.20)$$

where the subscripts b and s refer to the bottom and surface concentrations (mol cm^{-3}), respectively, and K_i is the Henry's law constant for each gas species (mol cm^{-3} atm^{-1}), and the bottom air flux is assumed to be zero. The diffusive flux is assumed to be driven by the concentration gradient across the entire depth of the surface-water body.

The aqueous concentrations of species at the surface are calculated to be in equilibrium with the atmosphere at 10°C, where $P_{CO2}{}^{atm}$, $P_{air}{}^{atm}$, and $P_{CH4}{}^{atm}$ = 3.12 x 10^{-4}, 1.97 x 10^{-6}, and 9.87 x 10^{-1} atm, respectively (see Table 4.3 for K_i values):

$$[CO_2]_s = P_{CO2}{}^{atm} K_{CO2} \qquad (4.21)$$

$$[CH_4]_s = P_{CH4}{}^{atm} K_{CH4} \qquad (4.22)$$

$$[air]_s = P_{air}{}^{atm} K_{air} \qquad (4.23)$$

Unknowns in mass balance equations are now bottom concentrations and E. The pressure condition at the sediment surface is:

$$P_{air} + P_{CH4} + P_{CO2} + P_{H2O} = P_z \qquad (4.24)$$

We can neglect P_{H2O} in Eq. 4.24 relative to the other volatile components and substitute Henry's law expressions to obtain

$$\frac{[CO_2]_b}{K_{CO2}} + \frac{[CH_4]_b}{K_{CH4}} + \frac{[air]_b}{K_{air}} = P_z \qquad (4.25)$$

where K_i values are for the P_z considered (Table 4.3). With the approximations $[CO_2]_s \ll [CO_2]_b$ and $[CH_4]_s \ll [CH_4]_b$, bottom concentrations from Eqs. 4.18-4.20 are substituted into Eq. 4.25 to yield:

$$\frac{m}{K_{CO2}D/z + E/P_z} + \frac{m}{K_{CH4}D/z + E/P_z} + \frac{(D/z)[air]_s}{K_{air}D/z + E/P_z} = P_z \qquad (4.26)$$

By neglecting the first term in Eq. 4.26 and replacing K_{CH4} and K_{air} with an average K value, an approximate solution for E can be obtained:

$$E = m + \left(\frac{D}{z}\right)[air]_s - \frac{P_z\,KD}{z} \tag{4.27}$$

Substitution of Eq. 4.27 into Eqs. 4.18-4.20 gives the bottom concentrations of species:

$$[CO_2]_b \cong \frac{m}{D/z + EK_{CO2}^{-1}P_z^{-1}} \tag{4.28}$$

$$[CH_4]_b \cong \frac{m}{D/z + EK_{CH4}^{-1}P_z^{-1}} \tag{4.29}$$

$$[air]_b \cong \frac{(D/z)[air]_s}{D/z + EK_{air}^{-1}P_z^{-1}} \tag{4.30}$$

The diffusive and ebullition fluxes, F^D and F^E, respectively, of CO_2 and CH_4 can then be calculated:

$$F_{CO2}^D = \frac{D}{z}\left([CO_2]_b - [CO_2]_s\right) \tag{4.31}$$

$$F_{CH4}^D = \frac{D}{z}\left([CH_4]_b - [CH_4]_s\right) \tag{4.32}$$

$$F_{CO2}^E = EK_{CO2}^{-1}[CO_2]_b P_z^{-1} \tag{4.33}$$

$$F_{CH4}^E = EK_{CH4}^{-1}[CH4]_b P_z^{-1} \tag{4.34}$$

We calculated F^D and F^E for (1) CO_2 and CH_4 where seepage of CO_2 and CH_4 occurs into a surface water body and $m_{CO2} = m_{CH4}$, (2) CO_2 where only seepage of CO_2 occurs, and (3) CH_4 where only seepage of CH_4 occurs. In each of these cases (Cases 1-3), we consider a water body with z = 50, 1000, and 10000 cm, low, medium, and high m_{CO2} and/or m_{CH4} values (see Table 4.4 for m_{CO2} and m_{CH4} values), and calculate the percent ebullition of total flux for the species that seep into the water body. The low, medium, and high fluxes used here correspond approximately to our low, medium, and high seepage fluxes calculated in our prior vadose-zone-related work (Oldenburg and Unger, 2003; 2004). For comparison, natural fluxes of CO_2 from plant and soil biological processes are approximately 10^{-9} mol cm^{-2} s^{-1} (10 μmol m^{-2} s^{-1}) efflux to 3×10^{-9} mol cm^{-2} s^{-1} (30 μmol m^{-2} s^{-1}) uptake (e.g., Baldocchi and Wilson, 2001). We present results for both CO_2 and CH_4 to demonstrate the contrast in their ebullition and diffusion flux rates that arises from their different solubilities in water.

Our results (Table 4.4) show that diffusion is important for transport of CO_2 to the atmosphere in water bodies up to 1000 cm deep and for m_{CO2} up to the medium values considered. At greater m_{CO2} or z, CO_2 is transported to the atmosphere almost entirely by ebullition. For CH_4, diffusion is only an important transport mechanism for shallow (50 cm) water bodies and low m_{CH4}, accounting for about half the total CH_4 flux. For cases where CH_4 seeps into deeper water bodies of (z = 1000 and 10000 cm) or m_{CH4} is elevated, ebullition accounts almost entirely for the CH_4 flux to the atmosphere. These differences between ebullition and diffusion fluxes for CO_2 and CH_4 are due to the greater solubility of CO_2 in water, relative to CH_4. In short, ebullition and bubble transport dominate the transport of sparingly soluble species.

Table 4.3. Henry's law coefficients (K_i) for different P_z values (Spycher, unpublished code).

z (m)	P_z (atm)	K_{CO2} (mol atm^{-1} cm^{-3})	K_{CH4} (mol atm^{-1} cm^{-3})	K_{air} (mol atm^{-1} cm^{-3})
Surface-50 cm	1	4.90×10^{-5}	1.98×10^{-6}	1.29×10^{-6}
1000	2	4.87×10^{-5}	1.98×10^{-6}	1.29×10^{-6}
10000	11	4.63×10^{-5}	1.92×10^{-6}	1.26×10^{-6}

K values are for 10°C. K_{air} is the average of K_{N2} and K_{O2}.

Table 4.4. Percentage of flux by ebullition relative to diffusion for CO_2 and CH_4 at various depths and flux proportions.

Case	z (cm)	m^{CO2} (mol cm^{-2} s^{-1})	m^{CH4} (mol cm^{-2} s^{-1})	% $F_{CO2}{}^E$	% $F_{CH4}{}^E$
1	50	4.59×10^{-11}	4.59×10^{-11}	4	49
1	1000	4.59×10^{-11}	4.59×10^{-11}	31	92
1	10000	4.59×10^{-11}	4.59×10^{-11}	45	95
1	50	4.59×10^{-10}	4.59×10^{-10}	32	92
1	1000	4.59×10^{-10}	4.59×10^{-10}	82	99
1	10000	4.59×10^{-10}	4.59×10^{-10}	89	100
1	50	4.59×10^{-9}	4.59×10^{-9}	82	99
1	1000	4.59×10^{-9}	4.59×10^{-9}	98	100
1	10000	4.59×10^{-9}	4.59×10^{-9}	99	100
2	50	9.18×10^{-11}	0	8	NA
2	1000	9.18×10^{-11}	0	49	NA
2	10000	9.18×10^{-11}	0	63	NA
2	50	9.18×10^{-10}	0	31	NA
2	1000	9.18×10^{-10}	0	90	NA
2	10000	9.18×10^{-10}	0	94	NA
2	50	9.18×10^{-9}	0	90	NA
2	1000	9.18×10^{-9}	0	99	NA
2	10000	9.18×10^{-9}	0	99	NA
3	50	0	9.18×10^{-11}	NA	68
3	1000	0	9.18×10^{-11}	NA	96
3	10000	0	9.18×10^{-11}	NA	98
3	50	0	9.18×10^{-10}	NA	96
3	1000	0	9.18×10^{-10}	NA	100
3	10000	0	9.18×10^{-10}	NA	100
3	50	0	9.18×10^{-9}	NA	100
3	1000	0	9.18×10^{-9}	NA	100
3	10000	0	9.18×10^{-9}	NA	100

4.6. Transport of Dissolved CO$_2$ in Surface Water

Transport of the dissolved fraction of CO$_2$ in surface water will occur by diffusive and dispersive processes in the aqueous phase. Flow occurs in typical surface waters such as rivers, lakes, estuaries, and shallow seas by combinations of gravity, wind, and tidal forcings (e.g., Fischer et al., 1979). Such motions are often turbulent involving a wide range of chaotic flow velocities over a range of length scales which lead to effective dispersion and mixing of dissolved species. Dispersion and mixing will periodically expose surface water to the atmosphere where it will potentially equilibrate with atmospheric CO$_2$ creating an effective outgassing that is equal to the leakage and seepage flux at the bottom at steady state. In lakes, mixing may be somewhat less than in rivers or coastal environments and vertical mixing may occur only once or twice a year, or in some special cases not at all (e.g., deep equatorial lakes, or lakes with permanent ice cover) (Goldman and Horne, 1983). In addition, the density of CO$_2$-saturated water is approximately 1% greater than that of pure water (Ennis-King and Paterson, 2003), creating the possibility of dissolved CO$_2$ producing a stable density stratification. However, in typical surface waters other than deep marine environments and certain kinds of lakes, flow forcings such as gravity, wind, and tides will dominate over density stratification and cause mixing on time scales much smaller than the objective sequestration time scale (hundreds to thousands of years). Thus we assert that rivers, lakes, estuaries, and continental shelf ocean water will not be effective at attenuating leakage and seepage fluxes of CO$_2$ occurring as a dissolved component. Furthermore, as we have shown in Section 4.5, ebullition will generally occur for the flux magnitudes of interest thus subordinating the importance of diffusion and dispersion to the overall transport of CO$_2$ leakage and seepage in surface water.

4.7. Effects of Pressure, Temperature, and Salinity on Ebullition

As shown by the differences in ebullition flux between CO$_2$ and CH$_4$ calculated in Section 4.5, the solubility of the volatile species is a fundamental control on ebullition. The solubility of CO$_2$ is a strong function of salinity and temperature, both of which may vary within the subsurface and surface waters through which leaking CO$_2$ can migrate. We have calculated CO$_2$ solubility for various H$_2$O-NaCl mixtures using the methods of Spycher and Pruess (2004) and Spycher et al. (2003). We consider the case of a 200-m-deep surface water body at 10 $^{\circ}$C and underlying porous media with a geothermal gradient equal to 30 $^{\circ}$C km^{-1} and hydrostatic pressure assuming ρ_{H2O} = 1000 kg m^{-3}. The various solubility profiles are plotted as a function of depth in Fig. 4.6. The curves on the left-hand side of Fig. 4.6 represent hypersaline brines such as might be found in a very deep brine formation, and a typical oilfield brine, approximately twice the salinity of seawater. These two curves are plotted only up to the sediment-water interface because they are normally found in the subsurface. The final two curves are those of seawater and freshwater and continue from subsurface through the surface water. The CO$_2$ density profile is calculated from the online NIST Webbook (Lemmon et al., 2004) for pure CO$_2$ at the given pressures and temperatures.

The first point to note in Fig. 4.6 is that CO$_2$ transitions from supercritical to liquid to gas as it rises upwards in this system. This is in stark contrast to the simple change from supercritical to gas (see Fig. 2.4) that occurs in the absence of surface water (Oldenburg and Unger, 2003). The

implication of these phase transitions is that buoyancy forces on CO$_2$ bubbles are nearly constant with a slight decrease as the bubble rises, for example from –1000 m to –380 m in Fig. 4.6. Then upon rising through the liquid-gas transition, the enormous density change in CO$_2$ will lead to approximately a factor of 3.7 change in volume of the bubble, assuming an isothermal transition, with corresponding increase in upward buoyancy force.

The second important point illustrated in Fig. 4.6 is the variation in CO$_2$ solubility upward from depth. At intermediate and low salinity, CO$_2$ solubility rises slightly along a bubble migration path upward from depth until the liquid-gas transition point (depth equal to –380 m). From this point upward, CO$_2$ solubility declines rapidly as the pressure falls. The implication of this pattern for bubble transport is that CO$_2$ ebullition is favored as dissolved CO$_2$ is transported upwards from depths shallower than approximately -380 m in this system.

Finally, Fig. 4.6 shows dramatically the variation in solubility as a function of salinity of water. This has important implications for situations where the migration pathway of CO$_2$ leakage and seepage can traverse formations and surface water with contrasting salinity. For example, consider first the case of a briny groundwater system at depth with overlying fresher aquifers below a freshwater lake. In this case, a rising CO$_2$ bubble would encounter water with progressively higher and higher CO$_2$ solubility, making it likely that CO$_2$ bubbles would disappear as the CO$_2$ dissolved into the aqueous phase. In contrast, there could be a system with fresh-water aquifers at depth underlying a shallow continental shelf marine environment. In this case, ebullition may become more important as salinity increases and pressure decreases as the CO$_2$ flux moves upwards. Combinations of the above transitions are of course possible, and Fig. 4.6 provides a general guide as to the trend toward greater dissolution or greater ebullition in water as a function of depth and salinity.

5. SUMMARY AND DISCUSSION

5.1. Summary

Our brief investigation and analysis of CO$_2$ leakage and seepage into surface water has resulted in the following main conclusions:

1. Numerous investigations have been conducted to measure natural CO$_2$ and CH$_4$ fluxes and concentrations in surface-water environments and to estimate the relative contributions of ebullition and dispersion to the total fluxes of these species to the atmosphere. These previous studies provide direct evidence of how CO$_2$ leakage and seepage fluxes of similar magnitude will behave, and they indicate that local conditions strongly control transport processes. Natural CO$_2$ and CH$_4$ fluxes and local concentrations are significant and can lead to ebullition making it challenging to discern leakage and seepage from natural emissions.

2. Prior studies of volcanic lakes that have undergone lethal CO$_2$ outgassing indicate that deep and stagnant conditions are conducive to the formation of waters that are supersaturated with respect to CO$_2$. Seasonal overturn, or other regular mixing processes such as natural convection by hydrothermal heating, neither of which occur at Lakes Nyos or Monoun may prevent extreme buildup of CO$_2$ and associated potentially lethal outgassing events.

3. Previous work in the areas of bubble physics and hydrostatics indicate that in order for a bubble to form, the sum of the partial pressures of the volatile components must exceed the local hydrostatic pressure and surface tension. Once a bubble forms and rises upwards, mass transfer occurs between the bubble and liquid.

4. Although Stokes Law is not formally applicable to gas-bubble rise in surface water for bubble sizes larger than approximately 0.1 mm, empirical data exist to predict bubble rise velocity over a wide range of bubble sizes. Bubble-rise velocity reaches a maximum of approximately 30 cm s^{-1} for bubbles approximately 0.7 mm in radius and declines for larger bubbles due to turbulence and related bubble oscillations.

5. In saturated porous media, e.g., below surface water, small CO_2 fluxes can be sustained by bubble flow especially in coarse and highly permeable porous media. For larger CO_2 fluxes, or finer porous media, transport is by channel flow.

6. Bubble-rise velocity in porous media has a maximum of approximately 18 cm s^{-1} in very coarse gravels. Bubble-rise velocity is much smaller in typical sediments, which can only sustain a small flux of CO_2 before transitioning to channel flow. CO_2 rise velocity in the channel-flow regime is governed by multiphase flow processes that can be studied using reservoir engineering simulation approaches.

7. Bubble-rise velocity for a liquid CO_2 bubble is slower than for a CO_2 gas bubble due to the much smaller density contrast between liquid CO_2 and water than between gaseous CO_2 and water.

8. For the range of seepage fluxes and surface-water depths considered in this study, CO_2 transport through the surface water will tend to be by ebullition/bubble flux for relatively high seepage fluxes and/or deep water bodies and by diffusion/dispersion for relatively low seepage fluxes and/or shallow water bodies. Species such as CH_4 with lower solubility in water are more likely to be transported by bubble flux.

9. As leaking CO_2 rises upwards, liquid-stable CO_2 phase conditions may be encountered, especially if there is overlying surface water. Therefore, CO_2 rising from depth will transition from supercritical to liquid to gas with upward rise. The transition from supercritical to liquid is not associated with a significant change in physical properties, (e.g., density, viscosity, solubility), while the transition from liquid to gas has large changes in properties and these changes favor bubble flow.

10. The solubility of CO_2 in water depends strongly on the *P*, *T*, and salinity conditions of water and the phase properties of the CO_2. Leaking CO_2 rising from depth through saturated porous media of varying salinity may tend to dissolve and/or undergo ebullition depending on the conditions. In general, CO_2 solubility decreases with depth at shallow depths, creating greater potential for ebullition as CO_2 rises upward into the near-surface environment.

5.2. Discussion

The results of our study allow us to make the following comments on the key research questions posed.

(1) What are the physical processes relevant to the migration through sediments and overlying surface water of CO$_2$ either as bubbles or as a dissolved component in water?

Bubbles are subject to buoyancy and surface tension forces in porous media, with surface tension dominating for fine porous media. CO$_2$ transport is likely to be by channel flow in the fine sediments below a surface-water body. These channels can be produced by bubble trapping and coalescence processes that arise in medium- and fine-grained porous media. Channels can also be created by the heterogeneity inherent in subsurface formations. Upon approaching the surface-water body as a second phase (gas or liquid), CO$_2$ bubbles will emanate from the sediment and rapidly rise upwards. Under this scenario, there is no ebullition process since the CO$_2$ already exists as a second phase in the porous media. Ebullition (i.e., bubble formation) at the interface of sediment and surface water and/or dispersive transport of CO$_2$ seepage from the sediment interface will only occur for seepage fluxes on the order of the background flux or smaller. For larger fluxes, channel flow and bubble flow are expected in the porous media and in the surface water, respectively. Dissolved CO$_2$ is transported by motions of the aqueous phase typically driven by gravity, wind, and tidal forcings.

(2) Does surface water attenuate or enhance CO$_2$ seepage flux?

Rising CO$_2$ bubbles are subject to mass transfer with surrounding waters, but the travel times are relatively short because rise velocities are high. In general, CO$_2$ bubbles, once formed, are expected to rise from the bottom to the top of typical surface-water bodies as solubility decreases with decreasing pressure. As for dispersion of dissolved CO$_2$, mixing times in surface waters are short relative to geologic CO$_2$ sequestration times, and dissolved CO$_2$ added by leakage and seepage is expected to exsolve rapidly from surface water as it mixes and equilibrates with atmospheric CO$_2$. Thus CO$_2$ seepage flux is not expected to be significantly attenuated by surface water.

(3) Under what conditions can CO$_2$ concentrations build up at depth and lead to the potential for catastrophic release?

Water becomes slightly denser when it contains dissolved CO$_2$. Lakes with deep stagnant regions subject to CO$_2$ fluxes from below are prone to stratification with water at depth that is supersaturated with CO$_2$ and subject to rapid outgassing if there is a disturbance to the lake that initiates overturn. Natural mixing processes such as seasonal overturn and wind-driven mixing—largely absent from the well known Lakes Nyos and Monoun—and man-made degassing schemes can be effective at preventing CO$_2$ buildup in deep stagnant lakes.

6. RECOMMENDATIONS FOR FUTURE RESEARCH

6.1. CO$_2$ Flow and Transport in Water

There are significant research needs in the area of leakage and seepage of CO$_2$ in saturated porous media and surface waters. We offer the following recommendations.

1. In our experience, there are limits to the amount of understanding and knowledge that theory and modeling can deliver. Actual field experiments invariably result in huge leaps of

understanding. We suggest that a small-scale, controlled CO_2 release experiment designed to simulate the migration of CO_2 upward from a deep source into the near-surface environment be carried out. One variant of the field experiment should be a case in which CO_2 bubbles up through saturated sediments into a shallow surface-water body. In the experiment, the form of CO_2 transport through the sediments, its seepage into surface water, and its transport upward through the surface water will be monitored visually along with various geochemical and air sampling approaches. We envision an experimental test site could be established to carry out these experiments in concert with the testing of various surface-monitoring approaches.

2. We have a very limited understanding of how CO_2 displaces water in porous media. This issue is relevant from small bubbles migrating upward, to channel flow of gas displacing water, to full multiphase flow of CO_2. We propose that a comprehensive experimental program be established to carry out bubble flow and relative permeability measurements of gaseous, supercritical, and liquid CO_2 flows in water-filled cores, artificial fractures, and other flow systems to establish credible relations that can be incorporated in models currently being used to simulate CO_2 leakage and seepage. These measurements are essential to our models, and we feel they have not been carried out to the extent needed.

3. Mass transfer from the bubble to the surrounding water is strongly controlled by the bubble-wall (i.e., interface) properties. Gas-liquid interfaces are well known for their tendency to attract impurities, biological material, and small particles. The extent to which mass transfer is affected by these materials and whether it stabilizes or destabilizes CO_2 bubbles rising in surface waters of various types has not been investigated. We suggest that an experimental program be developed to study CO_2 bubble mass transfer in surface water. This work would complement the analogous studies of CH_4 bubbles studies (e.g., Leifer and Patro, 2002).

4. The phase transitions and associated enthalpy changes that CO_2 undergoes during bubble rise will lead to temperature changes. We suggest that a simulation study be undertaken to investigate the degree of cooling that will be expected for the phase transitions (e.g., from liquid CO_2 in bubbles to gaseous CO_2 in bubbles) and related effects.

5. As with ground-surface seepage, geostatistical methods should be investigated for application to surface-water CO_2 leakage and seepage monitoring to discern leakage from natural background fluxes.

ACKNOWLEDGMENTS

NOMENCLATURE

A	empirical fit parameter	-
A$_d$	additional mass	-
d$_p$	porous media particle diameter	m
D	Diffusivity and dispersivity	m^2 s^{-1}
E	total ebullition rate	mol cm^{-2} s^{-1}
F$_B$	buoyancy force	N
F^D	diffusive flux	mol cm^{-2} s^{-1}
F^E	bubble (ebullition) flux	mol cm^{-2} s^{-1}
F$_d$	drag force	N
F$_E$	fraction ebullition flux	-
g	gravitational acceleration	m s^{-2}
H	Henry's Law coefficient	Pa
K	Henry's Law coefficient	mol cm^{-3} atm^{-1}
k	permeability	m^2
m	mole flux	mol cm^{-2} s^{-1}
n	porosity	-
N$_i$	molar content of gas species *i*	mol
q$_{Bi}$	bubble gas transfer rate of species *i*	mol cm^{-2} s^{-1}
P	pressure	Pa, atm
P$_{CO2}$	partial pressure of CO$_2$	Pa, atm
P$_{st}$	Surface tension pressure	N m^{-2}
P$_z$	hydrostatic pressure	Pa, atm
r	bubble radius	m
r$_p$	characteristic length scale of pore	m

R'	equivalent pore throat radius	m
R_b	bubble radius	m
u_b	bubble velocity	m s^{-1}
V_B	bubble velocity in surface water	m s^{-1}
z	vertical coordinate	m
ρ_g	gas-phase density	kg m^{-3}
ρ_f	fluid density	kg m^{-3}
σ	surface tension	N m^{-1}
θ	contact angle	degrees
[ ]	concentration	mol cm^{-3}

REFERENCES

Anderson, A.L. and W.R. Bryant, Gassy sediment occurrence and properties: northern Gulf of Mexico, *Geo-Marine Lett., 10*, 209-220, 1990.

Baldocchi, D.D., and K.B. Wilson, Modeling CO$_2$ and water vapor exchange of a temperate broadleaved forest across hourly to decadal time scales, *Ecological Modelling*, *142*, 155-184, 2001.

Boles, J.R., J.F. Clark, I. Leifer, and L. Washburn, Temporal variation in natural methane seep rate due to tides, Coal Oil Point area, California*, J. Geophys. Res., 106*, 27,077-27,086, 2001.

Brooks, M.C., W.R. Zise, and M.D. Annable, Fundamental changes in in-situ airsparging flow patterns, *Ground Water Monit. Rem.*, *19*(2), 105–113, 1999.

Casper, P., S.C. Maberly, G.H. Hall, and B.J. Finlay, Fluxes of methane and carbon dioxide from a small productive lake to the atmosphere, *Biogeochemistry, 49*, 1-19, 2000.

Chiodini, G., F. Frondini, D.M. Kerrick, J. Rogie, F. parello, L. Peruzzi, and A.R. Zanzari, Quantification of deep CO$_2$ fluxes from Central Italy. Examples of carbon balance for regional aquifers and of soil diffuse degassing, *Chem. Geol., 159*, 205-222, 1999.

Chiodini, G., F. Frondini, C, Cardellini, F. Parello, and L. Peruzzi, Rate of diffuse carbon dioxide Earth degassing estimated from carbon balance of regional aquifers: The case of the central Apennine, Italy, *J. Geophys. Res., 105*, 8423-8424, 2000.

Christensen, T.R., N. Panikov, M. Mastepanov, A. Joabsson, A. Stewart, M. Oquist, M. Sommerkorn, S. Reynaud, and B. Svensson, Biotic controls on CO$_2$ and CH$_4$ exchange in wetlands – a closed environment study, *Biogeochem., 64,* 337-354, 2003.

Corapcioglu, M.Y., A. Cihan, M. Drazenovic, Rise velocity of an air bubble in porous media: Theoretical studies, *Water Resour. Res.*, *40*, W04214, doi:10.1029/2003WR002618, 2004.

Ennis-King, J., and L. Paterson, Rate of dissolution due to convective mixing in the underground storage of carbon dioxide, in Gale, J., and Y. Kaya (eds.), *Proceedings of the 6th Intl. Conf. On Greenhouse Gas Control Technologies*, *Vol. 1*, p. 507-510, 2003.

Evans, W.C., M.L. Sorey, A.C. Cook, B.M. Kennedy, D.L. Shuster, E.M. Colvard, L.D. White, and M.A. Huebner, Tracing and quantifying magmatic carbon discharge in cold groundwaters: lessons learned from Mammoth Mountain, USA*, J. Volcanol. Geotherm. Res., 114*, 291-312, 2002.

Fischer, H.B, E.J. List, J. Imberger, and N.H. Brooks, *Mixing in Inland and Coastal Waters*, Academic Press, New York, 483 pp., 1979.

Giggenbach, W.F., Water and gas chemistry of Lake Nyos and its bearing on the eruptive process, *J. Volcanol., Geotherm. Res., 42*, 33-362, 1990.

Giggenbach, W.F., Y. Sano, and H.U. Schmincke, CO2-rich gases from Lakes Nyos and Monoun, Cameroon; Laacher See, Germany, Dieng, Indonesia, and Mt. Gambier, Australia-variations on a common theme, *J. Volcanol. Geotherm. Res., 45*, 3110323, 1991.

Goldman, C.R., and A.J. Horne, *Limnology*, McGraw-Hill, New York, 454 pp, 1983.

Halbwachs, M., Sabroux, J.-C., Grangeon, J., G. Kayser, J.-C. Tochon-Danguy, A. Felix, J.-C. Beard, A. Veilleveille, G. Vitter, P. Rishon, A. Wuest, and J. Hell, Degassing the "killer lakes" Nyos and Monoun, Cameroon, Trans. Am. Geophys. Union EOS, 281-285, 85(3), 27 July 2004.

Harriss, R.C. and D.I. Sebacher, methane flux in forested freshwater swamps of the southeastern United States, *Geophys. Res. Lett., 8*, 1002-1004, 1981.

Hornafius, S.J., D. Quigley, and B.P. Luyendyk, The world's most spectacular marine hydrocarbon seeps (Coal Oil Point, Santa Barbara Channel, California): Quantification of emissions, *J. Geophys. Res., 104*, 20,703-20,711, 1999.

Hovland, M., A.G. Judd, and R.A. Burke, Jr., The global flux of methane from shallow marine sediments, *Chemosphere, 26*, 559-578, 1993.

Iliuta, I, A. Ortiz-Arroyo, F. Larachi, B.P.A. Grandjean and Gwild, Hydrodynamics and mass transfer in trickle-bed reactors: an overview, *Chemical Engineering Science*, 54(21), pp. 5329-5337, 1999.

Ji, W., A. Dahmani, D.P. Ahfield, J.D. Lin, and E.Hill III, Laboratory study of air sparging: Air

flow visualization, *Ground Water Monit. Rem.*, *13*(4), 115–126, 1993.

Joyce, J. and P.W. Jewell, Physical controls on methane ebullition from reservoirs and lakes, *Env. Eng. Geosc., 9,* 167-178, 2003.

Keller, M.and R.F. Stallard, Methane emission by bubbling from Gatun Lake, Panama, *J. Geophys. Res., 99*, 8307-8319, 1994.

Leifer, I. And R.K. Patro, The bubble mechanism for methane transport from the shallow sea bed to the surface: A review and sensitivity study, *Continental Shelf Res., 22*, 2409-2428, 2002.

Leifer, I., J.F. Clark, and R.F. Chen, Modifications of the local environment by natural marine hydrocarbon seeps, *Geophys. Res. Lett., 27*, 3711-3714, 2000.

Lemmon, E.W., M.O. McLinden and D.G. Friend, "Thermophysical Properties of Fluid Systems" in NIST Chemistry WebBook, *NIST Standard Reference Database Number 69*, Eds. P.J. Linstrom and W.G. Mallard, March 2003, National Institute of Standards and Technology, Gaithersburg MD, 20899 (http://webbook.nist.gov).

Macdonald J.A., D. Fowler, K.J. Hargreaves, U. Skiba, I.D. Leith, and M.B. Murray, Methane emission rates from a northern wetland - response to temperature, water table and transport, *Atmos. Environ., 32*, 3219-3227, 1998.

de Marsily, G., *Quantitative Hydrogeology*, Academic Press, New York, 1986.

Martens, C.S. and J.V. Klump, Biogeochemical cycling in an organic rich coastal marine basin. 1. Methane sediment-water exchange processes, *Geochim. Cosmochim. Acta, 44*, 471-490, 1980.

Morel, F.M.M. and J.G. Hering, *Principles and Applications of Aquatic Geochemistry*, Wiley, New York, 1993.

Oldenburg, C.M., and A.J.A. Unger, On leakage and seepage from geologic carbon sequestration sites: unsaturated zone attenuation, *Vadose Zone Journal*, 2, 287-296, 2003.

Oldenburg, C.M., and A.J.A. Unger, Coupled Vadose Zone and Atmospheric Surface-Layer Transport of CO$_2$ from Geologic Carbon Sequestration Sites, *Vadose Zone Journal*, 3, 848-857, 2004.

Oldenburg, C.M., J.L. Lewicki, and R.P. Hepple, Near-surface monitoring strategies for geologic carbon dioxide storage verification, Lawrence Berkeley National Laboratory Report *LBNL-54089,* October 2003.

Oskarsson, N., Carbon dioxide bursts of lake Nyos, Cameroon, modeled as a periodic supersaturation in a countercurrent reactor, *J. Volcanol. Geotherm. Res., 42*, 307-318, 1990.

Pellicer, J., V. Garcia-Morales, and M.J. Hernandez, On the demonstration of the Young-Laplace equation in introductory physics courses, *Phys. Educ.*, *35*(2), 2000.

Roosevelt, S.E., and M.Y. Corapcioglu, Air bubble migration in a granular porous medium: Experimental studies, *Water Resour. Res.*, *34*(5), 1131–1142, 1998.

Rosenberry, D.O., P.H. Glaser, D.I. Siegle, and E.P. Weeks, Use of Hydraulic head to estimate volumetric gas content and ebullition flux in northern peatlands*, Water. Resour. Res., 39*, 1066, 2003.

Shipton, Z.K., J.P. Evans, B. Dockrill, J. Heath, A. Williams, D. Kirschner, and P.T. Kolesar, Natural leaking CO$_2$-charged systems as analogs for failed geologic sequestration reservoirs, In: Carbon Dioxide Capture for Storage in Deep Geologic Formations – Results from the CO$_2$ Capture Project, Volume 2: Geologic Storage of Carbon Dioxide with Monitoring and Verification; Elsevier Ltd., 2004a.

Shipton, Z.K., J.P. Evans, D. Kirschner, P.T. Kolesar, A.P. Williams, and J. Heath, Analysis of CO$_2$ leakage through "low-permeability" faults from natural reservoirs in the Colorado Plateau, east-central Utah, in Baines, S.J., and R.H. Worden (eds.), *Geological Storage of Carbon Dioxide*, Geol. Soc. London, *Special Publications*, *233*, 43-58, 2004b.

Sigurdsson, H., J.D. Devine, F.M. Tchoua, T.S. Presser, M.K.W. Pringle, and W.C. Evans, Origin of the lethal gas burst from Lake Monoun, Cameroun, *J. Volcanol. Geotherm. Res., 31*, 1-16, 1987.

Smith, L.K., W.M. Lewis, J.P. Chanton, G. Cronin, and S.K. Hamilton, Methane emissions from the Orinoco River floodplain, Venezuela, *Biogeochemistry*, *51*, 113-140, 2000.

Spycher, N., J. Ennis-King, and K. Pruess, CO$_2$-H$_2$O mixtures in the geological sequestration of CO$_2$. I. Assessment and calculation of mutual solubilities from 12 to 100 C and up to 600 bar. *Geochemica et Cosmochimica Acta*, *67*, 3015-3031, 2003.

Spycher, N, and K. Pruess, CO$_2$-H$_2$O mixtures in the geological sequestration of CO$_2$. II. Partitioning in chloride brines at 12-100 C and up to 600 bar, Lawrence Berkeley National Laboratory Report *LBNL-56334*, September 2004.

Torp T.A., and J. Gale, Demonstrating storage of CO$_2$ in geological reservoirs: The sleipner and SACS projects, *Energy, 29* (9-10), 1361-1369, 2004.

Walter, B.P. and M. Heimann, A process-based, climate sensitive model to derive methane emissions from natural wetlands: Application of five wetland sites, sensitivity to model parameters, and climate, *Global Biogeochem. Cycles, 14*, 745-765, 2000.

Wan, J, S. Veerapaneni, F. Gadelle, T.K. Tokunaga, Generation of stable microbubbles and their transport through porous media, *Water Resour. Res.*, *37*(5), p. 1173 (2000WR900331), 2001.

Washburn, L., C. Johnson, C.C. Gotschalk, and E.T. Egland, A gas-capture buoy for measuring bubbling gas flux in oceans and lakes, *J. Atm. Ocean. Technol., 18*, 1411-1420, 2001.

Wilson, J.O., P.M. Crill, K.B. Bartlett, D.I. Sebacher, R.C. Harriss, and R.L. Sann, Seasonal variation of methane emissions from a temperate swamp, *Biogeochemistry, 8*, 55-71, 1989.

Woods, A.W. and J.C. Philips, Turbulent bubble plumes and CO$_2$-driven lake eruptions, *J. Volcanol. Geotherm. Res., 92*, 259-270, 1999.
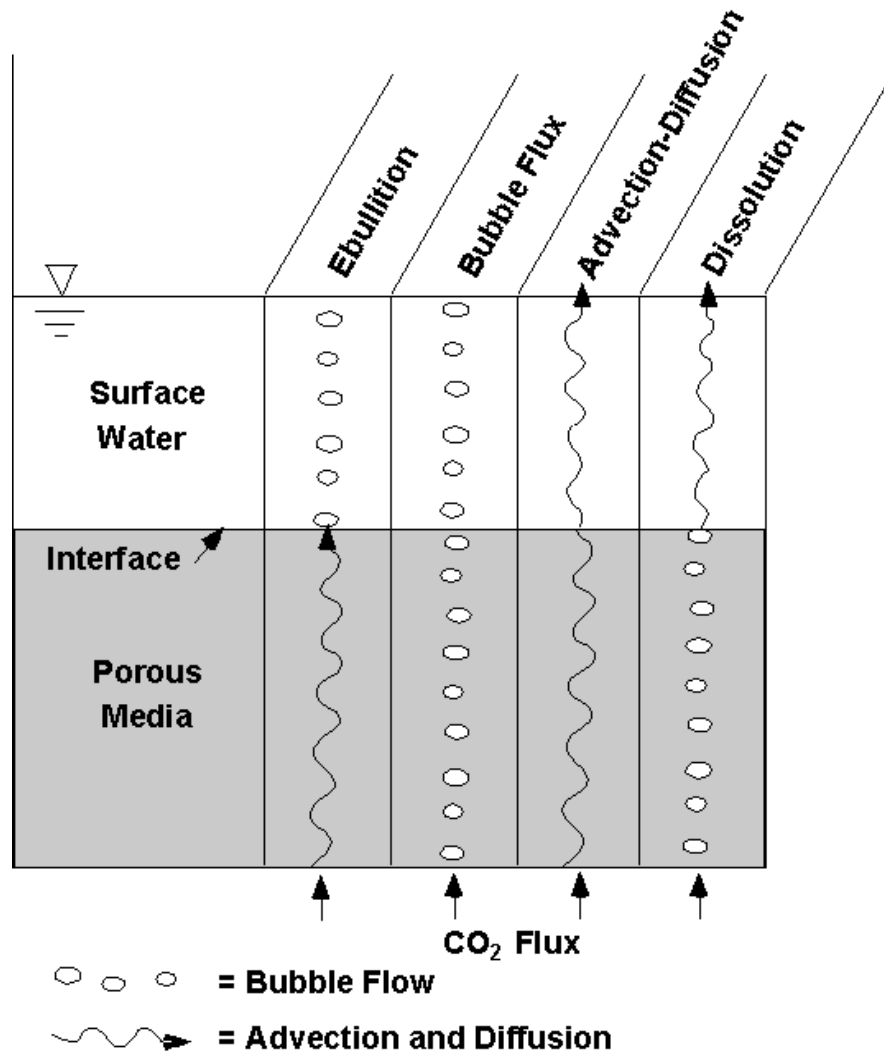
FIGURES

Figure 2.1. Schematic showing different combinations of coupled surface-water and porous media gas transport and transition at the interface between porous media and surface water.
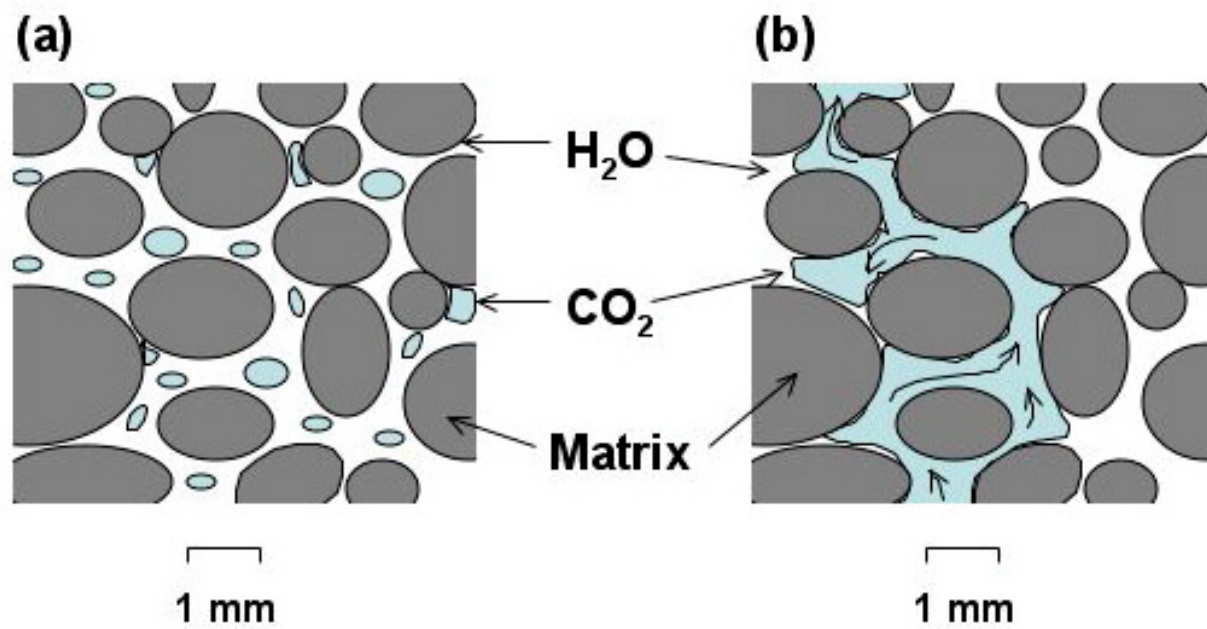
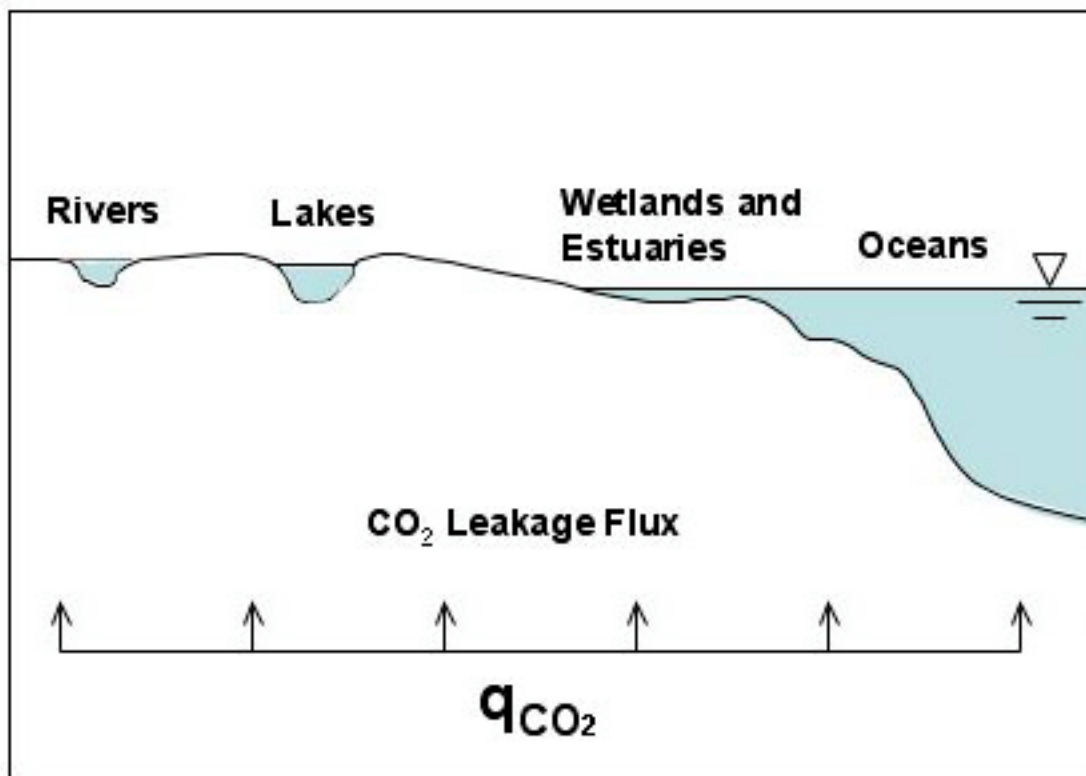*Figure 2.2. Schematic of flow regimes in porous media: (a) bubble flow, and (b) channel flow.*

Figure 2.3. Schematic of surface-water environments into which CO_2 leakage and seepage from geologic carbon sequestration sites may occur.
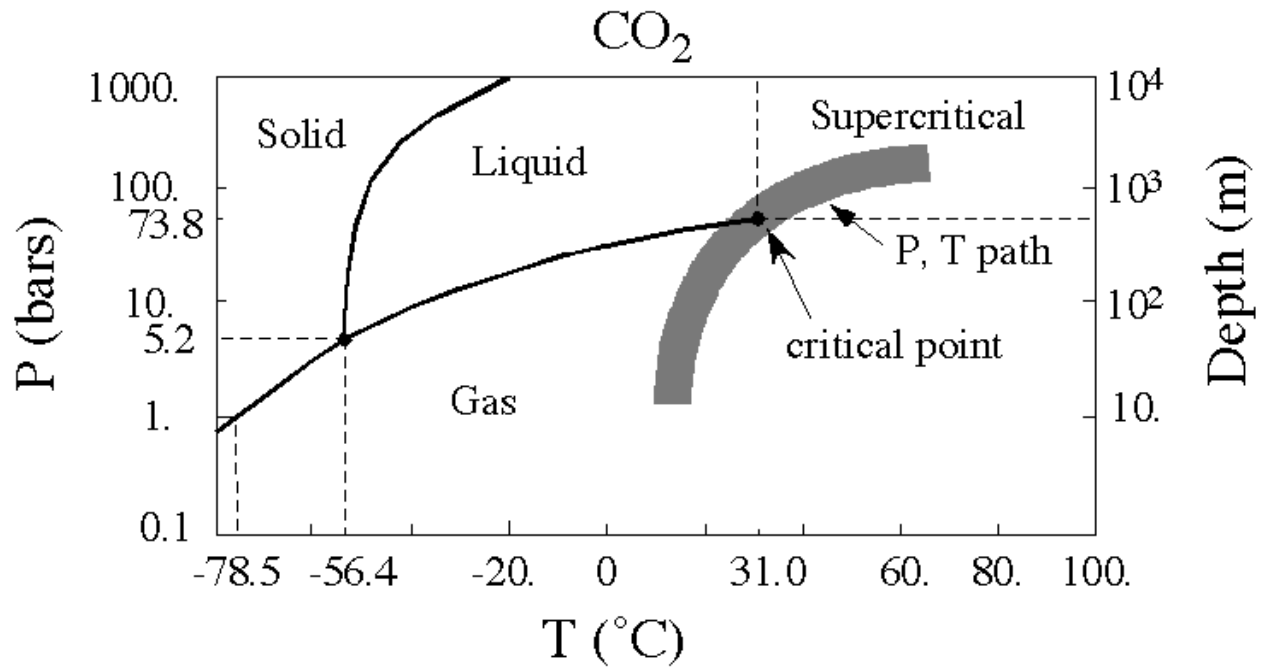
Figure 2.4. Phase diagram for CO$_2$ showing typical P-T *path with depth in the earth.*
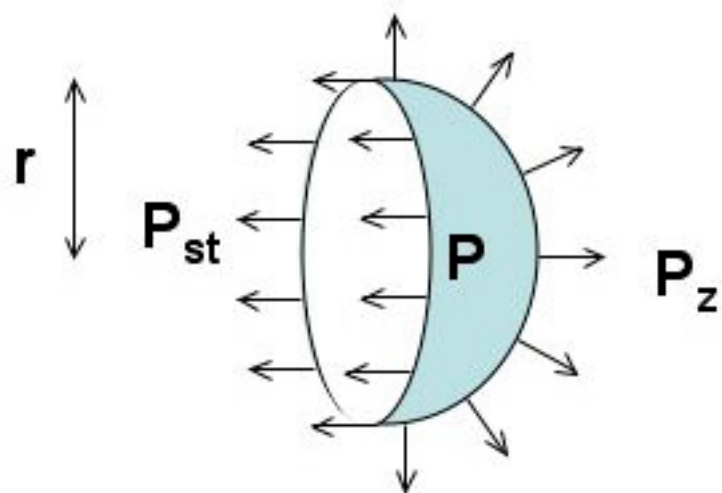
Figure 4.1. Half-section of a spherical bubble showing radiating forces due to pressure along with the surface tension forces due to P$_{st}$ along the equator. Pressure in the fluid is P$_z$, while pressure in the bubble is P.
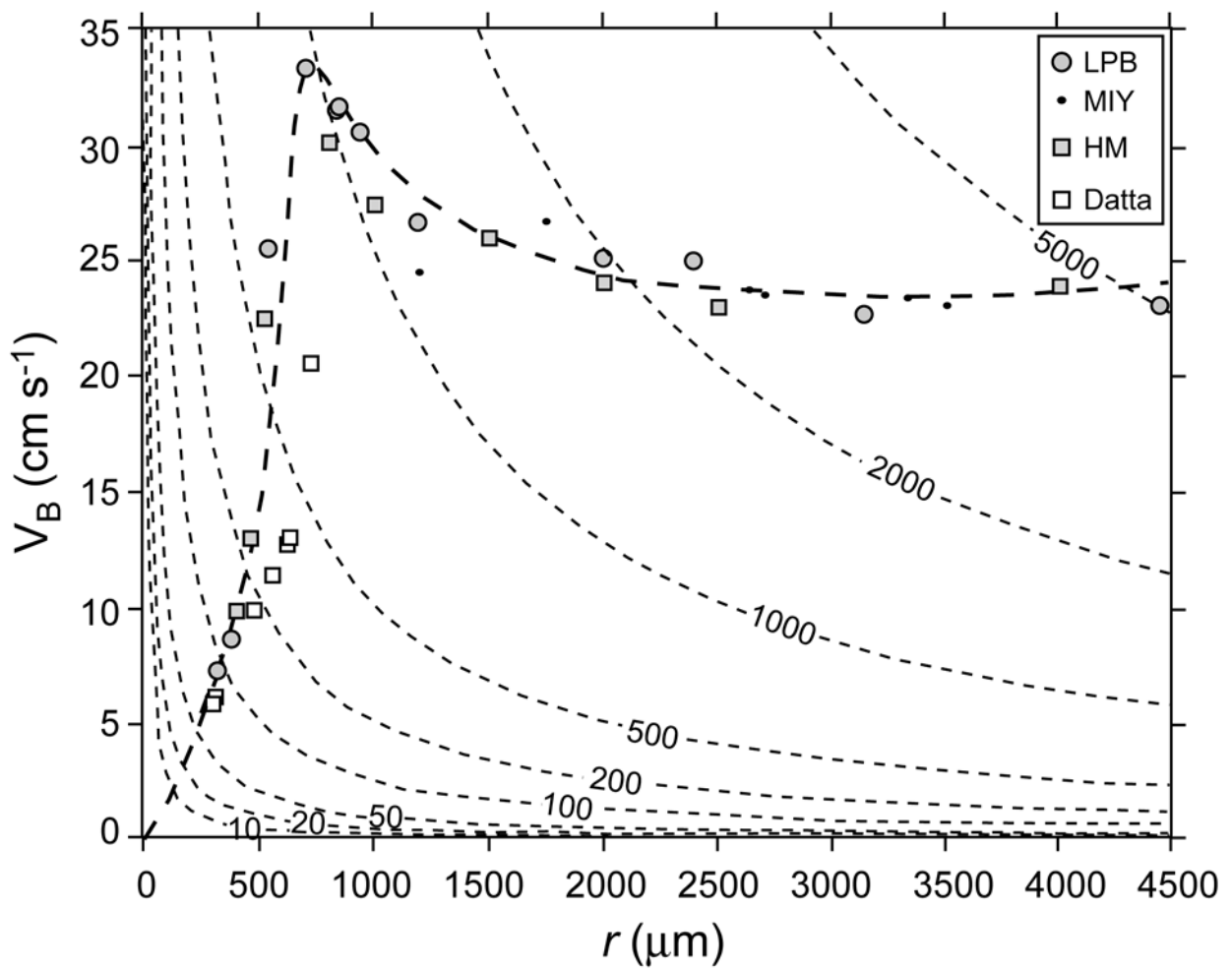
Figure 4.2. Bubble rise velocity as a function of bubble radius with background contours of Reynolds number (from Leifer and Patro, 2002).
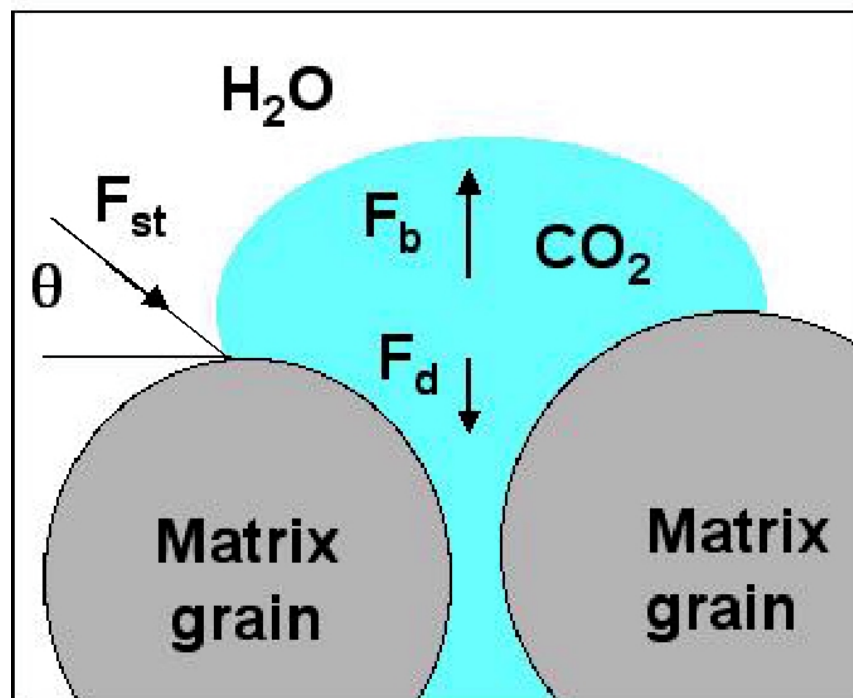
Figure 4.3. Force balance on single CO$_2$ bubble showing buoyancy force (F$_b$), drag force (F$_d$), and surface tension force (F$_{st}$) (after Corapcioglu et al., 2004).
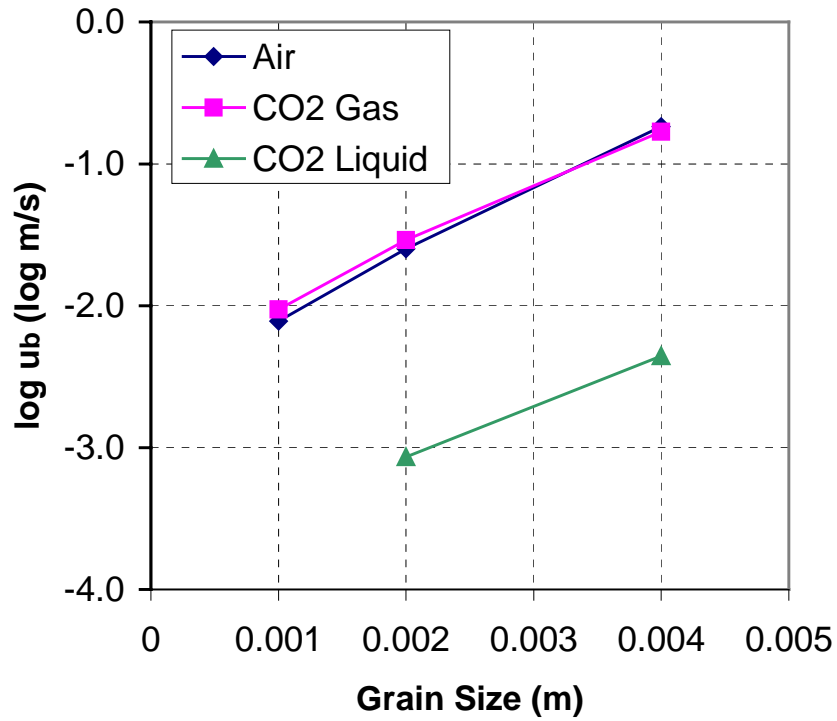
Figure 4.4. Log$_{10}$ u$_b$ for three different coarse porous media as a function of particle size.
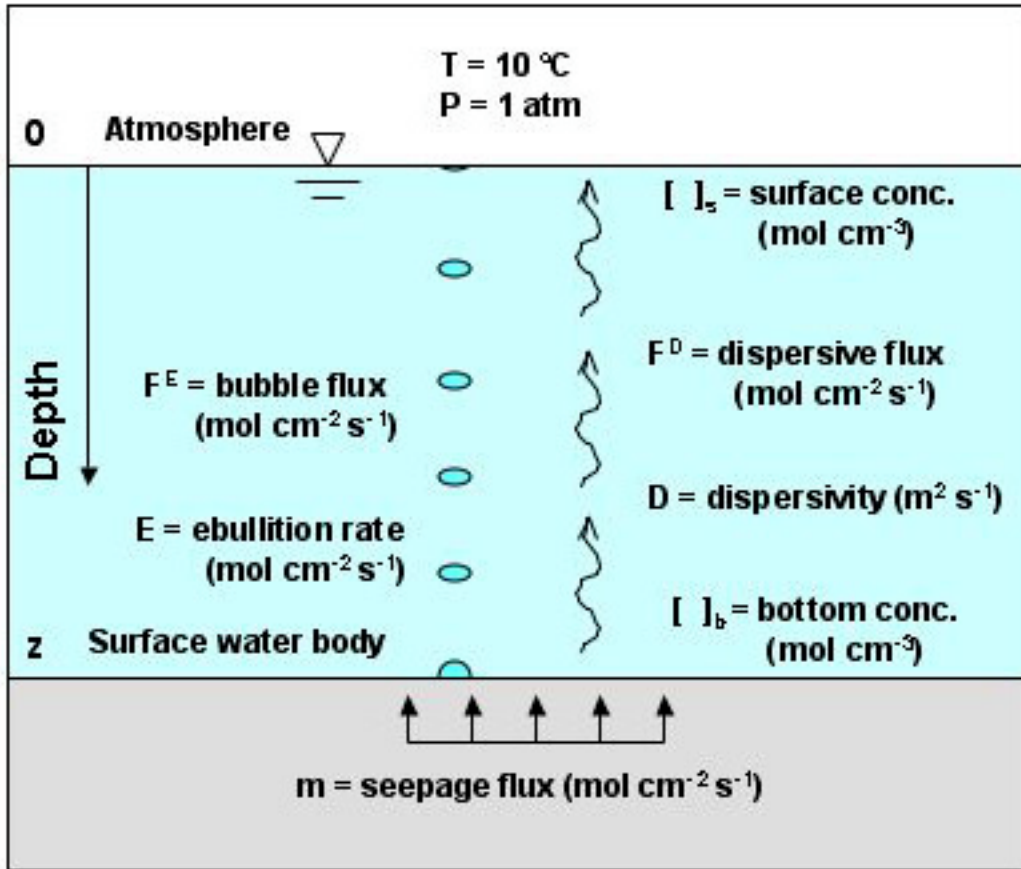
Figure 4.5. Schematic of domain and variables for ebullition vs. dispersive mass transport analysis. Ebullition is indicated by the bubbles, dispersion by the wiggly vector.
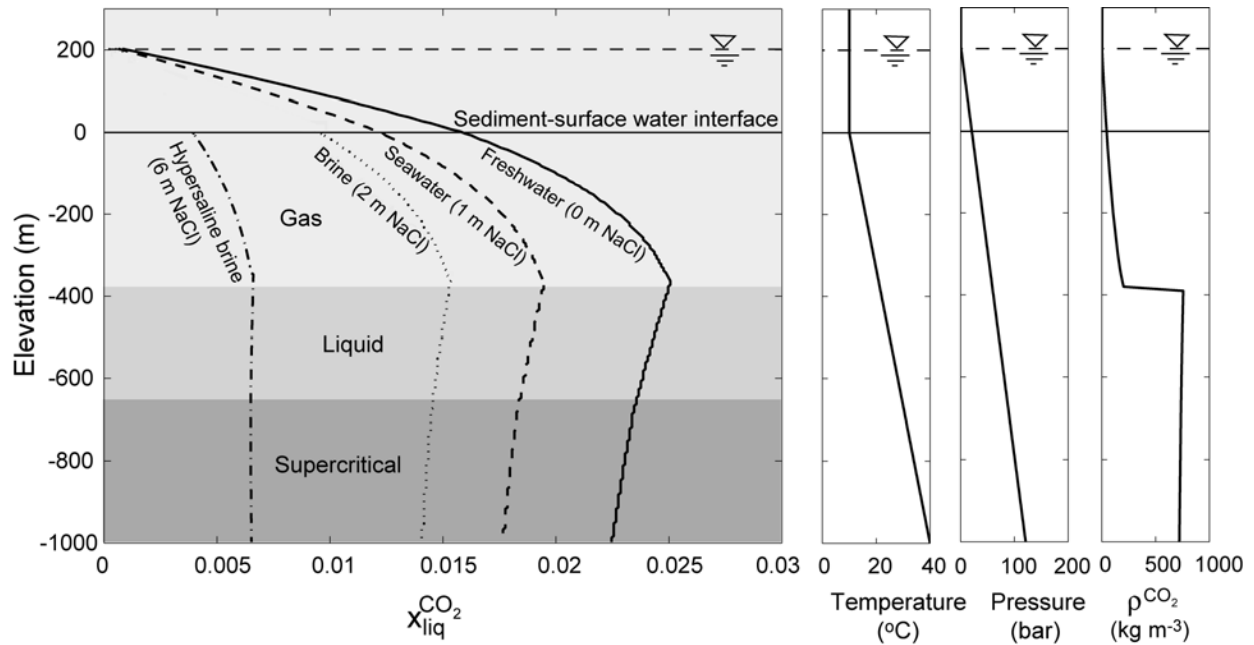
Figure 4.6. Solubility of CO$_2$ (mole fraction) and fully ionized salt in water and various brines as a function of depth within a surface water body (0-200 m) and the underlying formation (-1000 – 0 m) with the different phase stability fields for CO$_2$ indicated by the shading. Right-hand figures show corresponding temperature, pressure, and density of CO$_2$ with depth.